UCLA Samueli School of Engineering

Samueli Research Scholars

SURP 2021

UCLA SAMUELI SUMMER UNDERGRADUATE RESEARCH PROGRAM

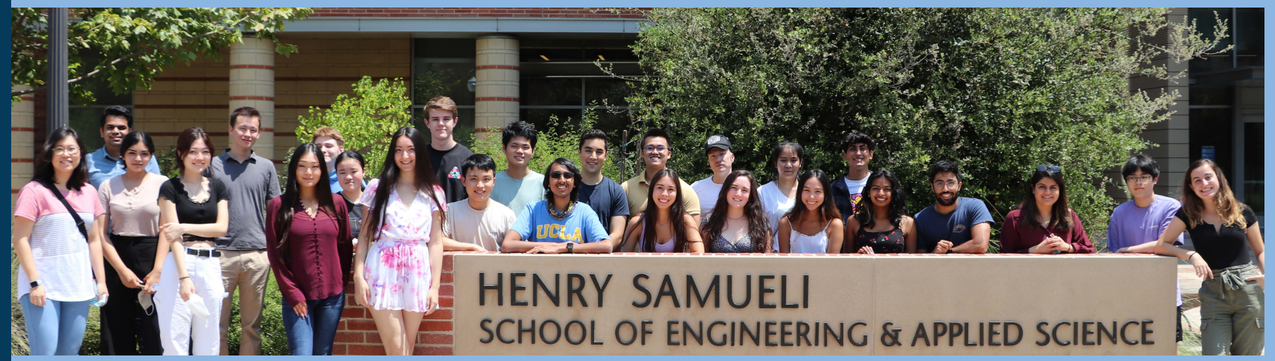

CONTENTS

DEAN'S MESSAGE

Ronald and Valerie Sugar Dean

The Summer Undergraduate Research Program (SURP) provides an intensive summer research experience in a wide range of engineering and physical science fields. Undergraduate students from all walks of life participate in research with UCLA Samueli School of Engineering faculty to gain real-world lab experience.

Due to the COVID-19 pandemic that is still affecting us this summer, SURP has had to transition the program into a remote learning environment for many of its scholars. Despite this challenge, SURP's many scaffolding resources and social events have still been able to occur and students were able to:

- Conduct research in a cutting-edge field at a world-renowned research institution.
- Meet and network with a community of peers who have similar goals and interests.
- Create a professional scientific poster and publish a research abstract.
- Learn to communicate research outcomes and present a detailed Summary of Project.
- Gain a competitive advantage for engineering graduate schools.
- Learn how you can impact your community as an engineer.

This year, a record 66 undergraduate students were selected to join the 2021 SURP cohort, spread out across 31 faculty in 6 engineering departments. We are happy to announce 64% of these are women, 20% are underrepresented minorities, and many are first generation and low income students. SURP is involved with ongoing efforts in fostering a more diverse, equitable and inclusive community at UCLA Samueli Engineering.

Creating new knowledge is a very difficult yet important task, and these high-performing students have done an outstanding job working through the rigors of academic research. These students should be very proud of all that they have accomplished in a short time this summer. I encourage you to explore our publication and learn about all the cutting-edge knowledge that is being created here.

Sincerely,

Dr. Jayathi Murthy
Ronald and Valerie Sugar Dean

Julia Bi

Electrical Engineering
Freshman, UCLA

Autonomous Vehicle with Offloaded Server Control using Mobile Edge Computing

FACULTY ADVISOR
C.K. Ken Yang

DAILY LAB SUPERVISOR
Jack Irish

DEPARTMENT
Electrical and Computer Engineering

ABSTRACT

Modern day mobile applications not only require a low latency, but but also incur a high energy cost. However, mobile devices are limited in their battery life and computational capabilities. Mobile Edge Computing (MEC) reduces latency and energy consumption by offloading some or all of the computing tasks to MEC servers. The Mobile Edge Compute Applications (MECA) lab establishes a 5G development environment that allows for experiments and testing with the 5G network and MEC. This particular project is an autonomous car controller which offloads control decisions to a central server, using a camera as input. Using gRPC, the camera sends images to the central server, which processes them and returns a control signal to guide the car. The goal is to compare the latency of this setup with traditional autonomous car controllers and achieve similar or better performance. At the moment, since it is difficult to gain access to physical materials, a simulation that imitates the complexity of video processing was used to gather data on the effectiveness of this strategy. As expected, sending the processing to a server is more time consuming with simple tasks, due to the initial time cost associated with the server-client communication. With more complex tasks, the server processing time is faster than processing at the client, since the server has better computational capabilities. The next step is applying these concepts to a physical setup with proper video processing and a car which takes the control signal.

UCLA Samueli School of Engineering

Autonomous Vehicle with Offloaded Server Control Using Mobile Edge Computing

Julia Bi, Jack Irish, Professor C.K. Ken Yang
Department of Electrical and Computer Engineering, University of California – Los Angeles

UCLA Samueli School of Engineering
SUMMER UNDERGRADUATE RESEARCH PROGRAM

Samueli Research Scholars
UCLA Samueli School of Engineering

FAST TRACK TO SUCCESS
UCLA Electrical and Computer Engineering

Introduction

The project aims to test concepts of Mobile Edge Computing (MEC), a technology that reduces latency and energy consumption of mobile devices through offloading computing tasks to external servers. Specifically, this concept was applied to an autonomous car that offloads decisions to a central server.

The goal is to measure the performance and latency of this setup, and compare it to traditional autonomous car controllers. We hypothesize that using MEC will allow the offloaded controller to have similar or better performance.

Background

Modern day mobile applications not only require a low latency, but also incur a high energy cost. However, mobile devices are limited in their battery life and computational capabilities.

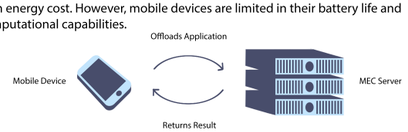

Figure 1: Mobile Edge Computing (MEC) solves this issue by offloading some or all of the computing tasks to MEC servers at the edges of mobile networks, therefore improving efficiency and reducing latency.

This project is an autonomous car controller which, instead of making decisions on the car itself like traditional controllers, offloads control decisions to a central server, which becomes more efficient as the computations become more complex. The car uses a camera as input. It streams video to the central server, which processes the video and returns a control signal.

Materials and Methods

Client-Server Communication:

To communicate between the camera, server, and car, the project uses gRPC. gRPC is Google's open source RPC (Remote Procedure Call) system that allows for bidirectional messages as well as streaming.

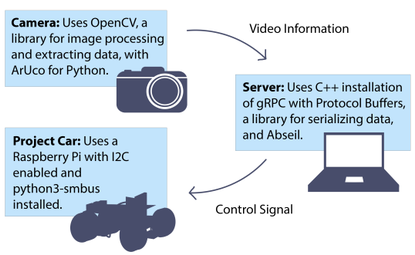

"Standard" Setup: The camera does the image processing and sends its results to the server, which then sends the results to the car. The image processing time is included in the camera-server latency.
"Streaming" Setup: The camera streams video directly to the server, which processes it and sends the result to the car. The image processing time is included in the server-car latency.

Results and Discussion

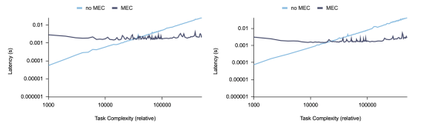

Figure 2: Task Complexity v. Latency Plots. Two simulations that imitate the complexity of video processing were used to gather data. As expected, server processing is more time consuming with simple tasks, due to the initial time cost of communication. With more complex tasks, the server processing time is faster because it has better computational capabilities.

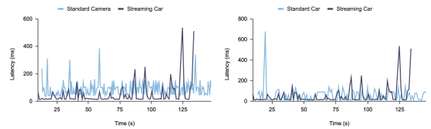

Figure 3: Time v. Latency Plots. *Left Plot:* The camera-server latency for the Standard setup and the server-car latency for the Streaming setup, both of which include the video processing, are plotted. The Streaming latency is on average lower than the Standard Latency by 39.2 ms, since the server has better computational capabilities. *Right Plot:* The server-car latencies for both the Standard and Streaming setup are plotted. The average latencies are roughly equal (Standard: 55.8 ms, Streaming: 49.3 ms), which is unexpected, since while their baseline latencies should be similar, the Streaming setup should be slightly slower on average because of the time taken by the server to do the image processing.

Conclusion

The relative efficiency of MEC vs Non-MEC in the simulation trials is as expected and confirms theory. The relative efficiency in the camera-car trials is somewhat unexpected and unclear, and should be investigated further.

Future Steps:

1. Further refine camera-car systems to stabilize latency measurements.
2. Gather and analyze data to explain unexpected results and confirm trends.

References

Gu, Xiaohui et al. "Energy-Optimal Latency-Constrained Application Offloading in Mobile-Edge Computing." Sensors (Basel, Switzerland) vol. 20,11 3064. 28 May. 2020, doi:10.3390/s20113064
https://pubmed.ncbi.nlm.nih.gov/32481742/

Mobile Edge Compute Applications Laboratory. https://mecalab.seas.ucla.edu

gRPC. https://grpc.io

Acknowledgements

I would like to thank Professor Yang and the MECA Lab, as well as the Samueli Engineering Summer Undergraduate Research Program and the Fast Track Program, for the support and resources. Many thanks to Jack Irish for his guidance and framework for this project. Many thanks to the Samueli Research Scholars Program for funding this research.

Gianna Brown

Bioengineering
Sophomore UCLA

How Implementing a Diverse Training Set Affects Skin Tone Bias in Deep Learning Algorithms

FACULTY ADVISOR

Achuta Kadambi

DAILY LAB SUPERVISOR

Pradyumna Chari

DEPARTMENT

Electrical and Computer Engineering

ABSTRACT

The COVID-19 pandemic has highlighted the growing need for avenues that will allow doctors to assess and treat their patients virtually rather than in person. One important component needed to implement telemedicine visits is the ability to take a person's heart rate virtually. Currently, there are algorithms that are able to do this by extracting ppg, which is the measure of blood flow under the skin. However, previous research has shown that their accuracy varies based on skin tone, with a much higher accuracy for lighter skin tones than darker ones. These inaccuracies need to be corrected before this technology is allowed to be used in the medical field in order to ensure equitable performance among all patients. Our lab attempts to minimize this bias by incorporating diverse training sets to train deep learning algorithms DeepPhys and PhysNet in order to determine the optimal proportion of lighter to darker skin tones in our training set needed to achieve an accurate ppg reading for all skin tones. Participants were asked to connect to a pulse oximeter and placed in front of a white background, while five one-minute videos were taken in sync with the pulse oximeter ppg readings. These videos were then used to train and test DeepPhys and PhysNet with different proportions of lighter skin tones to darker skin tones. Although the experiment is not yet complete, initial results show that having more darker skin participants in the training set decreases the accuracy of the networks in the testing set, but we believe that this is due to not having enough darker skin toned participants needed to truly test our hypothesis.

UCLA Samueli School of Engineering

How Implementing a Diverse Training Set Affects Skin Tone Bias in Deep Learning Algorithms

Gianna Brown, Pradyumna Chari, Oyku Deniz Bozkurt, Dr. Achuta Kadambi
Department of Electrical and Computer Engineering, University of California Los Angeles

UCLA Samueli School of Engineering
SUMMER UNDERGRADUATE RESEARCH PROGRAM

INTRODUCTION

Heart rate can be virtually measured through various algorithms, but previous research has shown that they are less accurate for darker skin tones. Our lab attempted to correct this bias by adjusting the training set of existing algorithms and finding the proportion of dark, medium, and light skin tones that need to be represented in the algorithm's training set in order to get accurate and unbiased results.

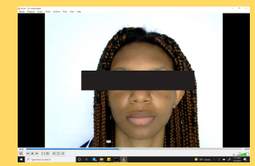

Figure 1 Screenshot from a video These videos are used to train deep learning algorithms DeepPhys and PhysNet before testing them on other videos within our database.

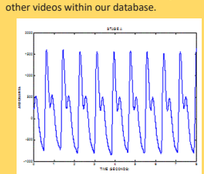

Figure 2 A ppg signal Deep Leaning algorithms can analyze the videos in order to find the ppg, which is the amount of blood flowing under the skin at a certain point in time. From there, it is easy to find the heart rate.

CONCLUSION

Although the experiment is incomplete, the initial results can give insight on how the study is going so far and if there is anything that should be changed to improve the study.

THINGS TO CONCLUDE

- So far, adjusting training set does not do well with addressing current disparities
- This may be due to underrepresentation of darker skin tone participants in data set

NEXT STEPS

- Work to ensure there are enough darker skin tone participants to successfully test the lab's hypothesis
- If this trend continues, look into other factors such as the construction of the algorithm or the background as possible sources of bias

MATERIALS AND METHODS

Figure 3 A picture of the experimental setup as described in Materials and Methods

Place participant in chair, adjust camera so that it is focusing on the face → Place pulse oximeter on participant's finger, wait until regular heart rate and ppg readings begin to come in → Extract heart rate and ppg values form the video and place in their own Excel sheet
Use the data from the videos and Excel sheets to train and test DeepPhys and PhysNet → Use Python code to take one minute video of participant while registering the heart rate and ppg values of each frame, repeat 5 times

Figure 4 The Fitzpatrick skin Type Scale After participant videos are collected, this scale is used to categorize a participant's skin tone a s light (Type 1 and 2), medium (Type 3 and 4) or dark (Type 5 and 6). The lab them selects an appropriate amount of each skin tone to be included in the training and testing sets.

RESULTS AND DISCUSSION

Although the experiment is not yet complete, the lab has enough data to begin training and testing to gather initial findings.

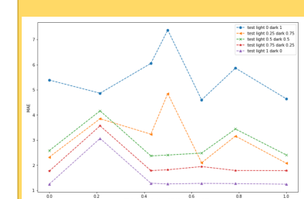

Figure 5 Results Graph This graph describes the mean absolute error of PhysNet based on the proportion of light to darker skin tone participants included in the training set

The graph to the left (Figure 5) shows the mean absolute error (MAE) of videos run through PhysNet trained with different training sets containing different proportions of light skin toned and dark skin toned participants.

IMPORTANT OBSERVATIONS

- Tests with more light skin participants fared better
- For tests with more dark skin participants, .2 light to .8 dark seems promising
- More representation of darker skin tones is needed before we can present conclusive results

ACKNOWLEDGEMENTS

I would like to thank Dr. Achuta Kadambi for allowing me into his lab and thank grad students Pradyumna and Deniz for mentoring me and helping me understand the project.

I would also like to thank the SURP program for mentoring me and providing me with workshops to allow me to learn how to format and share the research done over the summer.

REFERENCES

1 Taken from lab
2 https://www.researchgate.net/figure/PPG-signals-from-commercial-heart-rate-monitor-1_fig10_264622988
3 Taken from lab
4 https://www.skinrenewal.co.za/fitzpatrick-skin-type-iii
5 Taken from lab

Marisa Duran

Computer Science
Freshman, UCLA

Visual Processing for Autonomous Robot Swarms

FACULTY ADVISOR

Ankur Mehta

DAILY LAB SUPERVISOR

Ankur Mehta

DEPARTMENT

Electrical and Computer Engineering

ABSTRACT

Visual processing is an integral piece of robotic autonomy, as cameras attached to the robot collect and process pictures, allowing robots to sense the world around them. Robots collect information from the processed image and use it to make decisions. The goal of this project is to use colored blob detection and AprilTag detection to control low-cost robotic swarms, or cohesive groups of robots. I used an openMV camera, which is a small microprocessor with a camera attached, to accomplish this. To recognize colored blobs, I used thresholds to group pixels by color, which is a method that reduces issues with lighting changes. I programmed the camera to effectively recognize multiple different colored blobs at the same time and determine the distance between the camera and the object if the object's dimensions are known. The error associated with this calculation is about 20 millimeters from a range of less than a meter. AprilTags are recognized by the unique pattern of the tag, and I determined that the range of detection is dependent on the tag size. I used the AprilTag recognition capability to determine the relative position of the robot. The calculation of the distance between the camera and the tag has an average error of about 40 millimeters at a range of 3 meters, which is a relatively insignificant amount. We then applied these capabilities to robot swarm autonomy, using them to recognize a target object, calculate distances between robots, and perform other swarm behavior.works include using active cooling systems to increase thermal performance and conducting real-world magnetic tests with the PCB designs.

UCLA Samueli School of Engineering

Visual Processing for Autonomous Robot Swarms

Marisa Duran, Dr. Ankur Mehta
Laboratory for Embedded Machines and Ubiquitous Robots
UCLA Electrical and Computer Engineering Department

Samueli Research Scholars

UCLA Samueli School of Engineering
SUMMER UNDERGRADUATE RESEARCH PROGRAM

LEMUR

Objective: To use colored blob detection and AprilTag detection to control low-cost robot swarms

Introduction
- Visual processing provides robots with information that is used to make decisions
- In robot swarms, there is a need to find each robot's relative position
- I used AprilTags to determine the relative position
- I used colored blobs to identify other robots and target objects
- We then applied these capabilities to autonomous robot swarms

Key Terms
Computer Vision: When computers interpret information from images and videos
Feedback Control: When sensors on a robot (such as a camera) collect information and then robots take action based on that information
Robot Swarm: A group of robots that work together towards a common goal
Color Thresholding: A method that groups together similarly colored pixels, if they are within a certain constraint or threshold that represents a color

Detecting Colored Blobs and AprilTags

Materials

Figure 1: OpenMV Camera (left) connected to an ESP32 Featherboard (right)

Experimental Setup

Figure 2: Measuring reliability, range, and error of AprilTag detection

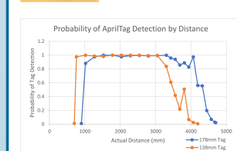

Figure 3: Graph displaying the range and reliability of AprilTag detection for differently sized tags

Using Vision to Control Robots: Methods

Colored Blob Detection (Figure 4)
- Recognizes multiple colors
- Achieved with color thresholding
- Finds blob position
- Calculates z-distance

Figure 4: Colored blob recognition

AprilTag Detection (Figure 5)
- Recognizes unique tags
- Finds relative position and orientation
- Calculates distance
- Reliable detection (see Figure 3)

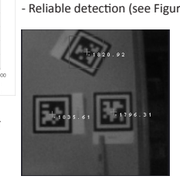

Figure 5: AprilTag recognition

Applying Visual Processing to Robots

Paper Boats (Figure 8)
- Detecting a colored cup

Paper Cars (Figure 6)
- Finding the location of a colored car
- Detecting AprilTags from above the car to determine the relative position

Blimps (Figure 9)
- Tracking a colored box

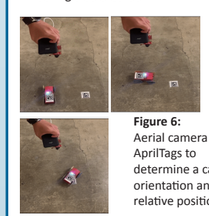

Figure 6: Aerial camera using AprilTags to determine a car's orientation and relative position

Limitations
- The AprilTag distance calculation has an associated error

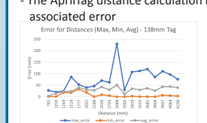

Figure 7: Graph displaying the error for the calculated distance

Camera = red arrow

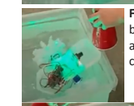

Figure 8: Paper boat tracking a red cup with color detection

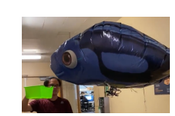

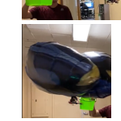

Figure 9: Blimp turning to follow a green box using colored blob detection

Acknowledgements

- Dr. Ankur Mehta
- Bhavik Joshi, Grace Kwak, Jillian Pantig, Sudarshan Seshadri, Jaehoon Song, Shahrul Kamil bin Hassan, and LEMUR
- William Herrera and the Summer Undergraduate Research Program
- Samueli Research Scholars

Conclusion

Visual processing provides many capabilities for autonomous robot swarms.
Colored Blob Recognition and AprilTag Recognition
- Recognizes landmarks, other robots, and target objects
- Determines distance between two robots
- Determines orientation

When integrated into a robot swarm, camera sensing and visual processing provides the robots with all the necessary information in order for the robots to work cohesively as a group.

Virginia Garcia

Chemical Engineering
Freshman, UCLA

Developing Predictive Abilities for Cancer Cell Growth

FACULTY ADVISOR
Jun Park

DAILY LAB SUPERVISOR
Kris Park

DEPARTMENT
Chemical Engineering

ABSTRACT

Cancer, being a leading cause of death, is a highly researched topic, yet researchers have struggled to understand the relationship between metabolism and cancer cell growth. Glycolysis and gluconeogenesis are the two most important pathways in cancer metabolism. In a low glucose environment, only gluconeogenesis can be performed. A challenge in analyzing cancer's metabolic pathways is measuring what happens inside cells. Cells are dynamic beings which reside in dynamic environments. Traditional measurement techniques are limiting because they rely on a snapshot of the cell and environment, which is a crude representation of the dynamic processes. In order to understand the internal workings, this project sought to measure metabolic fluxes and dynamic metabolic pathway usage. The approach involved conducting flux balance analysis within Cobra Toolbox. First, experimental measurements of cellular nutrient requirements and gene expression data from The Cancer Genome Atlas were mapped in Rstudio. By incorporating those experimental measurements, the human Recon3D model was tailored to model non-small cell lung cancer. Conducting flux balance analysis on the model using appropriate parameters will yield an approximate growth rate of lung cancer cells. Data collection has not yet been completed. This research is important because if it is possible to predict whether or not cancer cells can complete gluconeogenesis, specific therapies for distinct cancer cells can be developed. The predictive abilities that will be gained from completing this project will provide much needed insight into the dynamic systems of cancer cell growth.

UCLA Samueli School of Engineering

Developing Predictive Abilities for Cancer Cell Growth

LILLY GARCIA, KRIS PARK, JUN PARK

Samueli Research Scholars

UCLA Samueli School of Engineering

SUMMER UNDERGRADUATE RESEARCH PROGRAM

UCLA Samueli School of Engineering

INTRODUCTION

Cancer is a leading cause of death and a very important disease to understand. Yet, the dynamic nature of cells and their environment make them difficult to study. This project aims to better understand the dynamic nature of cells by measuring metabolite fluxes and predicting cancer cell growth rates.

APPLICATION

If it is possible to predict whether or not cancer cells can complete gluconeogenesis, specific therapies for distinct cancer cells can be developed.

KEY TERMS

- Tumor Microenvironment-Where Cells survive and proliferate. Different conditions can stifle or help growth
- Gluconeogenesis- Important pathway for Cancer cell growth in low glucose environment. Opposite of glycolysis with some exceptions
- Flux Balance Analysis (FBA)- Mathematical approach for predicting metabolic phenotypes, growth rates, and pathway utilization
- Recon3D- Genome scale model for the entire human body including protein and metabolite structure and atom-atom mapping

pyr
↓
glc

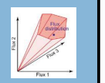

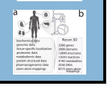

METHODS

1. Download Data from The Cancer Genome Atlas (TCGA) database
2. Determine gene expression patterns for Lung Squamous Cell Carcinoma in RStudio
3. Impose constraints on nutrient uptake
4. Complete FBA on Recon3D model in Cobra Toolbox to determine growth rate

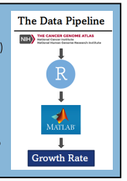

GOAL

- Develop predictive abilities of cancer cell growth using flux balance analysis
  - Predict which types of cancer can survive in low glucose environments
- Create better understanding of cancer metabolism
- Understand where to interfere in metabolic pathways in order to stop growth

RESULTS AND DISCUSSION

Modeling growth with FBA is possible for microbes

```
>> model=readCbModel('iAF1260.xml');
model=changeRxnBounds(model, 'EX_glc__D_e', -18.5, 'l');
model = changeRxnBounds(model,'EX_o2_e',-1000,'l');
model = changeObjective(model,'BIOMASS_Ec_iAF1260_core_59p81M');
FBAsolution = optimizeCbModel(model,'max');
FBAsolution.f

ans =

    1.7478
```

Figure 1: MATLAB code which establishes the lower bounds for glucose and oxygen exchange and maximizes the established objective reaction.

The E. coli model is one of the simplest model systems. Model iAF1260 can be found in the BIGG database and represents a strain of E. coli. After loading the model into MATLAB, Cobra Toolbox was used to change constraints of specific reactions within the model and maximize the flux rate of the Biomass reaction. The growth rate was found to me 1.7478 hr^-1, which corresponds to a doubling time of 0.3966 hours, a reasonable doubling time for this strain. Therefore, modeling growth with FBA was successful for E. coli.

It is possible to incorporate experimental data

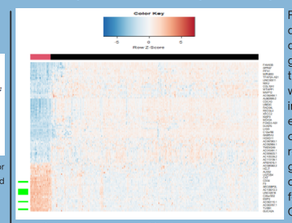

Figure 2: Heat Map generated in RStudio showing gene expression patterns of Lung Squamous Cell Carcinoma based on patient data.

From the TCGA patient data, the 100 most differently expressed genes were mapped and their fold change values were identified. This information was exported to MATLAB in order to find associated reactions for metabolic genes. Experimental data of gene expression for Lung Squamous Cell Carcinoma was successfully complied for use with the Recon3D model.

Gene-Protein-Reaction Associations

	1 Protein Name	2 Gene ID	3 Fold Change Value	4 rxn1	5 rxn2	6 rxn3	7 rxn4	8 rxn5	9 rxn6
1	"GPD1"	"2819_AT1"	0.0169	"r0202"	"G3PD1ir"	"G3PD2"	[]	[]	[]
2	"HSD17B6"	"8630_AT1"	0.0493	"HMR_2041"	"HMR_6633"	[]	[]	[]	[]
3	"NPR1"	"4881_AT1"	0.0487	"GUACYC"	[]	[]	[]	[]	[]
4	"CA4"	"762_AT1"	0.0076	"HCO3Ee"	"HCO3E"	"GMAND"	[]	[]	[]
5	"SLC6A4"	"6532_AT1"	0.0064	"SRTRN6_2_r"	[]	[]	[]	[]	[]
6	"GGTLC1"	"92086_AT1"	0.0046	"GTHRDH_syn"	"GGTAm2"	"r0648"	"r0641"	"r0649_1"	[]
7	"ABCA8"	"10351_AT1"	0.0274	"TCHOLABCtc"	"ESTRAABCtc"	"ESTRSABCtc"	"LEUKABCtc"	[]	[]
8	"AK1"	"203_AT1"	0.1628	"DADK"	"HMR_0765"	"HMR_6545"	"FBP"	"FBP26"	"ADK1"
9	"PLA2G1B"	"5319_AT1"	0.0108	"PLA2_2e"	[]	[]	[]	[]	[]

Table 1: This table represents the Gene-Protein-Reaction Associations between the most differently expressed genes in Lung Squamous Cell Carcinoma and reactions in the Human Recon3D model. It also includes associated Fold Change Values which were found in Rstudio.

We are continuing to tailor this approach to the Recon3D model

```
%% Setting initial constraints

%sets the lower bound of all exchange reactions that are not initially 0 to
%be -0.0074
ind1=find(model.lb~=0)&(~cellfun(@isempty,strfind(model.rxns,'EX_')));
model.lb(ind1)=-0.00074;

%sets the lower bound of all sink and demand reactions to be 0
ind2=find(~cellfun(@isempty,strfind(model.rxns,'DM_')));
model.lb(ind2)=0;
ind3=find(~cellfun(@isempty,strfind(model.rxns,'SK_')));
model.lb(ind3)=0;

%based on the given constraints, maximizes the
%flux rate of the Biomass reaction
model=changeObjective(model,'BIOMASS_reaction');
FBAsolution = optimizeCbModel(model,'max');
Ei= FBAsolution.f;
doubling_time1=log(2)/Ei;
```

```
Ei =
    0.0289

doubling_time1 =
   24.0185
```

Figure 3: MATLAB code which sets lower bounds of Sink and Demand reactions equal to 0 and the lower bounds of all exchange reactions that are not 0 to be -0.0074. It then finds the flux rate of the objective reaction.

The Recon3D model has been set up to represent healthy tissue. The lower bounds have been so that the doubling time of the objective reaction is about 24 hours. The next step will be to integrate the experimental data and to determine which amino acids have the most effect of the growth rate, especially in low glucose environments.

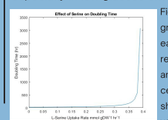

Figure 4: Example of the graphs that will be made for each amino acid to represent the effect of amino acid exchange rate on cell growth rate. This graph shows Serine exchange rate vs. doubling time

CONCLUSION

Because the experiment has not been competed, it is unclear whether experimental data paired with FBA is enough to be able to predict cancer cell growth rates. This experiment showed that it is possible to predict growth rates for microbes and it is possible to incorporate experimental data, but more research is necessary to know if this approach is viable with more complex models such as the Human Recon3D model.

FUTURE GOALS

- Integrate this approach with lab experiments in order to verify the model, and use it to guide experiments. These experiments include using isotope tracing and LCMS to measure
  - nutrient uptake rates
  - cell growth rates
  - intercellular flux
- Refine this computational approach enough to have predictive power for individual patients solely based on a tumor biopsy and rna-sequencing

ACKNOWLEGEMENTS

- Thank you to the Samueli Research Scholars for choosing me to participate in Research
- Thank you to Will Herrera and SURP for academic, career and research guidance
- Thank you to Kris Park for the technical support
- Thank you to Doctor Jun Park for the guidance, support, and encouragement

Sources:

Brunk, E., Sahoo, S., Zielinski, D. C., Altunkaya, A., Dräger, A., Mih, N., Gatto, F., Nilsson, A., Preciat Gonzalez, G. A., Aurich, M. K., Prlić, A., Sastry, A., Danielsdottir, A. D., Heinken, A., Noronha, A., Rose, P. W., Burley, S. K., Fleming, R., Nielsen, J., Thiele, I., … Palsson, B. O. (2018). Recon3D enables a three-dimensional view of gene variation in human metabolism. Nature biotechnology, 36(3), 272–281. https://doi.org/10.1038/nbt.4072

Kahn, Daniel. "Introduction to Flux Balance Analysis". http://ibis.inrialpes.fr/people/dejong/courses/coursINSA/2016/Introduction_to_FBA

Murfin, Kelley. "3 Things to Know about the Tumor Microenvironment." MD Anderson Cancer Center, MD Anderson Cancer Center, 6 Apr. 2021, www.mdanderson.org/cancerwise/what-is-the-tumor-microenvironment-3- things-to-know.h00-159460056.html.

Sahiti Gavva

Chemical Engineering
Freshman, UCLA

Thermodynamic Simulations Using Industrial Waste Streams for CO2 Mineralization

FACULTY ADVISOR
Dante Simonetti

DAILY LAB SUPERVISOR
Steven Bustillos

DEPARTMENT
Chemical Engineering

ABSTRACT

CO_2 mineralization is a viable alternative CO_2 emissions mitigation strategy in which CO_2 is captured by the precipitation of thermodynamically favorable carbonate phases. For CO_2 mineralization, industrial waste streams with large cation concentrations (e.g., Ca^{2+} [0.01 - 1.0 mol/L]) react with dissolved CO_2 under alkaline conditions (pH > 9). An ion-exchange process has previously been proposed to provide the alkalinity required for CO_2 mineralization while utilizing industrial waste streams. In this work, thermodynamic simulations were performed using Gibbs Energy Minimization Selektor (GEMS) program to predict yields and purities of calcite ($CaCO_3$) formed. The alkaline solution produced via ion-exchange and industrial waste streams were simulated to predict the final compositions of the solution to see how the final composition would affect the overall process. Industrial waste stream compositions were identified using the United States Geological Survey database. Simulations were performed at varying CO_2 concentrations (100%, 50% 20%, 12%, 5%) at fixed waste stream compositions to quantify the effect CO_2 concentrations have on calcite yields, purities, and final solution compositions. The data collected shows acceptable yields (0.14 - 1.3 g/L calcite) and purities (>90%) for calcite using industrial waste streams at each respective CO_2 concentration. Final divalent cation concentrations were predicted following treatment via nanofiltration and reverse osmosis, which resulted in total divalent cation concentrations less than <0.001 mol/L. The low divalent cation concentrations following mineralization and the large yields and purities of calcite simulated confirm that the overall mineralization process is viable using industrial waste streams.

UCLA Samueli School of Engineering

THERMODYNAMIC SIMULATIONS USING INDUSTRIAL WASTE STREAMS FOR CO_2 MINERALIZATION

Sahiti Gavva, Steven Bustillos, Professor Dante Simonetti
Department of Chemical Engineering at University of California, Los Angeles

UCLA Samueli School of Engineering
SUMMER UNDERGRADUATE RESEARCH PROGRAM

Introduction

Today's emissions, specifically CO_2, have terrible consequences on the globe. Emissions need to be prevented or captured to prevent further damage. While there are other ways to prevent or capture emissions, mineralization proves promising because of the stability of minerals and their potential profitability.

Figure 1: The overall process for mineralization. Steps of the process are defined below.

Bubbling Chamber: Dissolving CO_2 in water, produces an acidic solution.

Ion Exchange Column: Uses resin and zeolites to increase pH and form carbonate ions (CO_3^{2-}) needed in reaction.

Reactor: Minerals are formed with the carbonate ions and Produced Water (PW). Produced Water stream refers to industrial waste streams that are rich in cations needed for the mineralization reaction.

Mineral Filter: A vacuum filter is used to separate any minerals formed.

Nanofiltration: Removes any unreacted divalent ions with 95% efficiency.

Reverse Osmosis: Separates water from any remaining ions.

- The water is reused in the bubbling chamber, and
- the other stream, which is rich in Na^+, is reused in the Ion Exchange Columns to prep the resins and zeolites for reaction to increase pH and form carbonate ions.

Mineralization Reaction

$$Ca^{2+}_{(aq)} + CO_3^{2-}{}_{(aq)} \rightarrow CaCO_{3\,(s)}$$

- Thermodynamically favorable; reactions happens spontaneously
- Process has the potential to be integrated in a power plant without requiring extra money or energy.

Calcite, or more commonly limestone, is used in building materials, such as cement and can be further expanded to other processes depending on purity.

Objective

It is important to understand if the mineralization process is viable for power plants. The objective of this research is to simulate the mineralization reaction to predict if highly pure calcite could be formed at a large yield and if filtration of leftover ions would allow for regeneration.

Materials & Methods

Gibbs Energy Minimization Selektor (GEMS) software

- Simulates reaction between the Carbonate and Produced Water streams
- Predicts formation and yields based on initial inputs, allowing for the minerals formed and unreacted ions to be analyzed.

Method

Run simulation for a specific PW composition and CO_2 concentration.

Graph yields of calcite and purities of calcite against the amount of PW.

Calculate the concentration of leftover ions after nanofiltration and reverse osmosis.

Repeat for other CO_2 concentrations.

References

Bustillos, Steven, Alturki, Abdulaziz, Prentice, Dale, La Plante, Erika Callagon, et al. (2020) Implementation of Ion Exchange Processes for Carbon Dioxide Mineralization Using Industrial Waste Streams. *Frontiers in Energy Research. 8.* https://www.frontiersin.org/article/10.3389/fenrg.2020.610392

Results

Using waste stream data from the United States Geological Survey (USGS), the values of ions was averaged to produced a Produced Water composition (Figure 2) which was run through the GEMS simulation to predict the calcite produced and the ions leftover.

	Concentration (mmol/L)
$CaCl_2$	20.7
NaCl	339.2
$MgCl_2$	7.5
$FeCl_2$	0.28
KCl	3.15
$CaSO_4$	1.68

Figure 2: Produced Water Composition in mmol/L that was input into GEMS.

Figure 3: The amount of calcite formed with varying levels of CO_2 concentration. The focus is the peak of each curve (the max amount of calcite produced).

Figure 4: The percentage of calcite formed out of total minerals formed. The focus is, again, the point where amount of calcite produced peaks (from Figure 3).

20% CO_2

	Initial (mmol/L)	Filtered (mmol/L)
Na^+	91.630	164.934
Ca^{2+}	0.411	0.041
Mg^{2+}	1.802	0.180

12% CO_2

	Initial (mmol/L)	Filtered (mmol/L)
Na^+	60.748	109.346
Ca^{2+}	0.474	0.047
Mg^{2+}	1.202	0.120

Figure 5: Concentration of leftover ions predicted by GEMS and calculated concentration of ions after nanofiltration (95%) and reverse osmosis in mmol/L.

Discussion

Yield	Purity	Filtered Ions
Good	Highly pure	Ideal for the regeneration stream of Na^+
Ranges from 0.14 – 1.3 g/L calcite for CO_2 concentrations	greater than 90% when calcite yield is at its peak for all CO_2 concentrations.	Ion concentration of Ca^{2+} and Mg^{2+} are less than 1 mmol/L after filtration. The leftover ions in Figure 5 are reflective of the leftover ions for the other CO_2 concentrations not show in the table.

The mineralization process appears to reliably produce calcite with acceptable yield and purity. With little leftover ions after filtration, the regeneration streams of Na^+ and fresh water are also practical for the process.

Conclusion

By producing calcite, a significant amount of CO_2 can be captured. This process enables power plants to decrease their emissions generated, instead producing minerals that could be used elsewhere.

Future Directions

1. Further Validate Experimentally: This data will confirm the viability of mineralization on power plants.
2. Secondary Mineralization: Using the ion concentrate that is produced as a waste product of nanofiltration, a secondary reaction may produce a significant amount of mineral, allowing the process to capture more CO_2.

Acknowledgements

Samueli Engineering Summer Undergraduate Research Program

Women in Engineering at UCLA

Steven Bustillos (DLS)

Professor Dante Simonetti (PI)

Vanessa Huaco

Chemical Engineering
Freshman, UCLA

Analysis of Scattering Data Using Bayesian Optimization

FACULTY ADVISOR
Samanvaya Srivastava

DAILY LAB SUPERVISOR
Divya Iyer

DEPARTMENT
Chemical Engineering

ABSTRACT

Polyelectrolyte complexation between oppositely charged macromolecules is primarily driven by non-covalent (electrostatic) interactions. These self-assembled materials find applications as bio-adhesives, encapsulants, delivery and purification agents. Analytical techniques such as small angle x-ray scattering (SAXS) and dynamic light scattering (DLS) offer insights about the size, structure and behavior of these materials, all of which are influenced by the polymer backbone, intermolecular interactions and solution conditions. In this project, we focus specifically on obtaining size and structure estimates of these materials via light scattering measurements, to explain structure-property relationships. We propose a Bayesian optimization model that will best describe and fit the size and structure estimates found. We are working to fit our equation

$$P(q) = (9 * scale * V * \Delta\rho^2) * \left[\frac{sin\,(qr) - qrcos(qr)}{(qr)^3}\right]^2$$

for a spherical model to our data. We are looking at the relationship between their form factor $(P(q))$ and length scale (q), where the form factor is the dependent variable, and the length scale is the independent variable. Our model will be constructed using the Statistics and Machine Learning toolbox in MATLAB, as well as the Parallel Computing toolbox. The effectiveness of toolboxes offered by MATLAB, to perform Bayesian Optimization, was tested with preexisting generic examples. The terms involved in the optimization process have been learnt and understood.

UCLA Samueli School of Engineering

ANALYSIS OF SCATTERING DATA USING BAYESIAN OPTIMIZATION

Samueli Research Scholars
UCLA Samueli School of Engineering

Vanessa Huaco, Divya Iyer, Professor Samanvaya Srivastava
Chemical and Biomolecular Engineering Department -
University of California, Los Angeles

UCLA Samueli School of Engineering
SUMMER UNDERGRADUATE RESEARCH PROGRAM

INTRODUCTION

Polyelectrolyte complex coacervates are unique polymer-rich materials that can serve many purposes but are yet poorly understood.[1]

Analytical techniques such as small angle x-ray scattering (SAXS) and dynamic light scattering (DLS) offer insights about the size, structure and behavior of these materials, all of which are influenced by the polymer backbone, intermolecular interactions and solution conditions.

Prior research utilizes Bayesian methods to analyze small angle scattering data of these materials. Understanding the properties and behaviors of these materials will help us harness self-assembly as a tool for material design.

OBJECTIVE

We aim to find the model that best fits and explains the size and structure estimates data obtained experimentally so that we may harness self-assembly as a tool for material design.

KEY TERMS

Small Angle X-Ray Scattering

A technique for studying structural features of colloidal size[2]

Dynamic Light Scattering

A technique in physics that can be used to determine the size distribution profile of small particles in suspension or polymers in solution

Bayesian Regression Analysis

A statistical process for estimating the relationships between a dependent variable and one or more independent variables in which the hypothesis is updated as more data becomes available

MATERIALS

MATLAB
- Statistics and Machine Learning Toolbox
- Parallel Computing Toolbox

METHOD

- Obtain scattering curves from SAXS and DLS
- Input data into MATLAB and preprocess the data set
- Partition Data and Remove Outliers
- Use curve fitting tools to find regression model that fits or data

RESULTS

Sphere model : $P(q) = I(q)/V = (9 * scale * V * \Delta\rho^2) * \left[\frac{sin\,(qr) - qrcos(qr)}{(qr)^3}\right]^2$

Equation inputted into MATLAB: $I(q) = a * r^3 [\frac{sin(qr) - qrcos(qr)}{(qr)^3}]^2$

a = 1.978e-05
r (radius) = 104.9
r-square = 0.9927

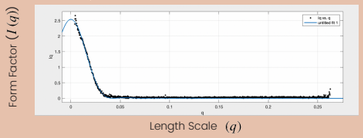

DISCUSSION

We utilized the curve fitting application in MATLAB to try and fit our equation for a sphere model to our data set. This resulted in the blue line displayed in the graph above. This model also gave us the value of the "a" coefficient and the value of the radius.

This fit yielded an r-squared value of 0.9927 which is a relatively good value, indicating that this is an okay fit for our data. However to obtain a customized equation that would better explain different datasets, especially in the low q region, which is the area of interest we must further refine our model using Bayesian Optimization.

CONCLUSION

- Regression Analysis and Bayesian Optimization were learnt and understood
- Effectiveness of MATLAB toolboxes were tested using generic examples
- Curve fitting tools were utilized to generate a model for our data

Further Steps:
- Extend this process to spherical systems
- Optimize our equations by building our own Bayesian algorithm
- Find the model that best fits and explains the size and structure estimates

References

[1] "Srivastava Lab." Research, www.srivastava-lab.net/research.
[2] Glatter O; Kratky O, eds. (1982). Small Angle X-ray Scattering. Academic Press. ISBN 0-12-286280-5. Archived from the original on April 21, 2008
[3] Kline, Steve, and Alan Munter. "Sphere Model." NIST Center for Neuron Research , ncnr.nist.gov/resources/sansmodels/Sphere.html.

Acknowledgments

I would like to thank the Samueli Research Scholars for funding our research through the Summer Undergraduate research Program. I would also like to thank Professor Srivastava, Divya Iyer and Holly Senebandith for their resources, guidance and support. Finally, I would like to thank Will Herrera and the SURP staff for putting together this program.

Tricia Jain

Civil and Environmental Engineering
Freshman, UCLA

Development of a Relational Database for Seismic Response Data from Instrumented Buildings Subjected to Historical Earthquakes

FACULTY ADVISOR
Henry Burton

DAILY LAB SUPERVISOR
Eusef Abdelmalek-Lee

DEPARTMENT
Civil and Environmental Engineering

ABSTRACT

The instrumentation of buildings with measuring devices, such as accelerometers, enables rapid assessments of building damage and functionality following an earthquake. However, in a typical urban context, only certain buildings are instrumented due to the associated costs. Fortunately, statistical and machine learning methods can utilize the response data collected from a limited number of sensors to predict seismic demands in uninstrumented structures. Currently, there exists a large inventory of seismic response data, but no standardized system of organization, hindering data analysis. As a result, this study seeks to develop a relational database to streamline the storage and retrieval of seismic response data, along with associated building and earthquake parameters. An efficient database schema, which eliminates data redundancy and simplifies links between tables, was designed. Appropriate data types for attributes, particularly vectors of time-series data, were researched and implemented. Code to accurately extract, organize, and insert over 2.5 GB of remote sensing data into the database was written. Finally, Python scripts were designed to enable data querying and analysis of extracted results. The relational database and accompanying python scripts that were developed create the framework for performing advanced data analysis. In the context of this dataset, this can improve post-earthquake building damage assessments, mitigating the socio-economic toll of earthquakes on communities.

UCLA Samueli School of Engineering

UCLA Samueli School of Engineering
SUMMER UNDERGRADUATE RESEARCH PROGRAM
Samueli Research Scholars

Development of a Relational Database for Seismic Response Data from Instrumented Buildings Subjected to Historical Earthquakes

Tricia Jain, Eusef Abdelmalek-Lee, Henry Burton Ph.D., S.E.
Department of Civil and Environmental Engineering— University of California, Los Angeles

Introduction

- The instrumentation of buildings with measuring devices enables rapid assessments of building damage and functionality following an earthquake.
- In a typical urban context, only certain buildings are instrumented.
- Statistical and machine learning methods can utilize the response data collected from a limited number of sensors to predict seismic demands to uninstrumented structures.

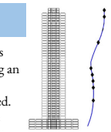

Figure 1. Measured Seismic Response

Objective

- Develop a relational database to streamline the storage and retrieval of seismic response data along with associated building and earthquake parameters.
- Design Python scripts to execute queries and analyse the extracted data.

Relational Database

- Utilizes tables to store data, which are related through shared fields (foreign keys).
- Reduces data redundancy and provides better scalability.
- Data extraction is performed by executing queries, which are requests for data.

Materials and Methods

- Designed and revised the database schema
- Introduced a junction table to reduce data redundancy
- Selected the MEDIUMTEXT data type to store time-updated data vectors

Extracted and wrote scalar value data into spreadsheets

Exported vectors of time-updated data into individual text files

Generated SQL statements for data insertion

- Implemented the database schema
- Ran queries to insert data into the database
- Performed tests for insertion accuracy

Created a notebook of example queries to facilitate database use

Performed statistical analysis of data using Python machine learning libraries

Published the database

Conclusion

- A relational database facilitates access to and analysis of large inventories of remote sensing data, providing the foundation for advanced data analysis.
- The DesignSafe cyberinfrastructure allows the greater natural hazards community to utilize the database in their research.
- The database can be continually updated with data from new earthquakes to better calibrate models.

Acknowledgements

I would like to thank Professor Burton and Eusef Abdelmalek-Lee for their guidance throughout this project, the Samueli Research Scholar Award for funding this research, and all SURP staff for their support.

Database Schema

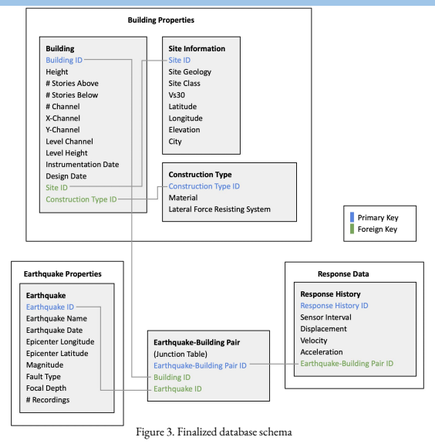

Figure 3. Finalized database schema

Results

Specifying columns to select information from

```
SELECT
    building.ID AS "Building ID",
    construction_type.LFRS AS "Lateral Force Resisting System",
    building.num_stories_above AS "Number of Stories Above Ground",
    building.num_chanel AS "Number of Sensors"
FROM
    construction_type
    JOIN
    building ON construction_type.ID = building.construction_type_ID
WHERE
    LFRS = 'Steel Moment Frame'
    AND num_stories_above > 10;
```

Tables to join

Join condition

Filtering parameters

Figure 4. Example query

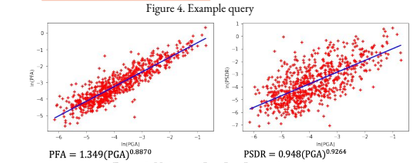

$PFA = 1.349(PGA)^{0.8870}$ $PSDR = 0.948(PGA)^{0.9264}$

Figure 5. Univariate Log-Log Regression

$$PFA = a(PGA)^b(S)^c$$

Figure 6. Multivariate Log-Log Regression Equation

References

Brandenberg, Scott J., et al. "Next-Generation Liquefaction Database." Earthquake Spectra, vol. 36, no. 2, May 2020, pp. 939–959, doi:10.1177/8755293020902477.
Omoya, Morolake; Ero, Itohan; zaker esteghamati, mohsen; Burton, Henry; Brandenberg, Scott; Nweke, Chukwuebuka (2021) "Relational database for post-earthquake damage and recovery assessment: 2014 South Napa earthquake." DesignSafe-CI. https://doi.org/10.17603/ds2-3nvj-4127.
Sun, H, Burton, H, Wallace, J. Reconstructing seismic response demands across multiple tall buildings using kernel-based machine learning methods. Struct Control Health Monit. 2019; 26:e2359. https://doi.org/10.1002/stc.2359
Zaker Esteghamati, Mohsen & Lee, Jeonghyun & Musetich, Matthew & Flint, Madeleine. (2020). INSSEPT: An open-source relational database of seismic performance estimation to aid with early design of buildings. Earthquake Spectra. 10.1177/8755293020919857.

Kim Kha

Mathematics
Junior, Mount Saint Mary's

Enoch Huang

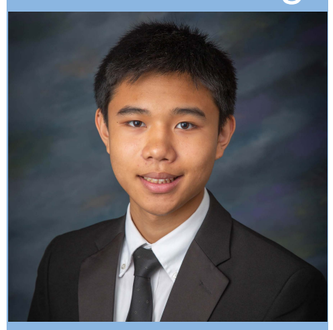

Electrical Engineering
Freshman, UCLA

Amanda Hacker

Electrical Engineering
Freshman, UCLA

Wearable & Mobile Bioanalytical Technologies for Personalized Medicine

FACULTY ADVISOR

Sam Emaminejad

DAILY LAB SUPERVISOR

Hannaneh Hojaiji

DEPARTMENT

Electrical and Computer Engineering

ABSTRACT

Exponential growth in Internet of Things (IoT) devices and wearable sensing technologies has created an unprecedented opportunity to enable personalized medicine through real-time individual biomonitoring. Although these commercialized platforms are capable of tracking physical activities and vital signs, they fail to access molecular-level biomarker information which provide insight into the body's dynamic chemistry. Thus, as sweat is a rich source of biomarkers that can be retrieved unobtrusively, sweat-based wearable biomonitoring has emerged as one of the most promising candidates to merge this gap. By designing and integrating compact electrochemical sensors into wearable electronic devices, we can non-invasively and accurately track specific biomarkers in sweat and provide actionable feedback about users' health status. We develop a signal modulation strategy to stimulate our electrochemical sensors for wearable biomarker monitoring. We also design a novel sensor readout methodology for improved and accurate biomarker tracking. Then, we integrate these designs into a wireless electrochemical readout circuitry to noninvasively track intended biomarkers. As a result, we successfully demonstrate our signal modulation solution's efficacy through electrodeposition of prussian blue films. Additionally, we show this sensing methodology improves signal readout and sensitivity by 3 times. Thus, we can non-invasively track subjects' biomarkers and underlying health status in a wireless and wearable format. This platform can further be utilized for real-time glucose monitoring in diabetic patients without requiring conventional painful extraction methods, or monitoring lithium levels in bipolar patients for drug abuse/compliance.

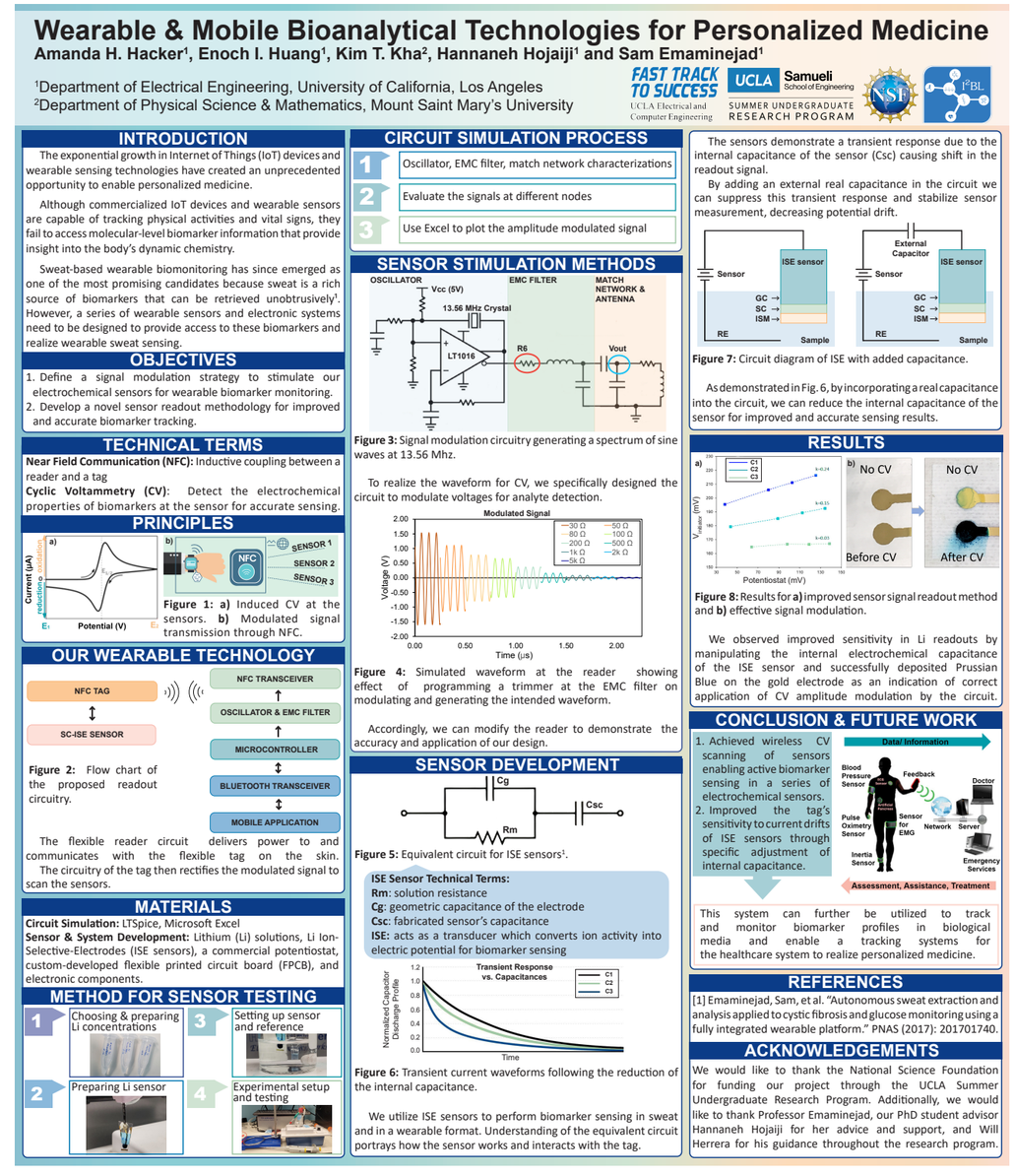

Ella Levine

Chemical Engineering
Freshman, UCLA

Annual Energy Output for Multijunction Solar Cells In Los Angeles County

FACULTY ADVISOR

Carissa Eisler

DAILY LAB SUPERVISOR

Lindsey Parsons

DEPARTMENT

Chemical Engineering

ABSTRACT

Implementing renewable energy sources is necessary to combat climate change. Typical solar panels use single junction cells (which use one material to absorb and convert light) instead of more expensive multijunction cells (which use multiple materials and convert sunlight more efficiently). Annual power production estimations are often based on efficiency, representing the power converted for a standard spectrum (AM1.5G), without accounting for spectral changes due to climate and season. These changes significantly impact annual energy generation, but data constraints and geographic variations hamper effective modeling. We hypothesized that a multijunction cell design employing a low-cost flat concentrator would generate significantly more energy from rooftop installations than current estimations of efficiency improvements. We applied Warmann's[1] spectral binning method and data from Los Angeles to detailed balance calculations with realistic concentrator and cell properties to predict the power output. Then, we applied developable residential roof area to calculate LA's annual solar energy generation for households. We found that our dual-junction solar cell design is 39.5% efficient while the record silicon single junction cell is 26.8% efficient. However, when accounting for annual spectral changes for LA, our design has a yearly maximum energy production of 472 kWh/m²—which is only 6.14% higher than the silicon cell (445 kWh/m²). This is lower than the percent increase in efficiency (47%). This demonstrates the importance of comparing designs through annual energy produced rather than efficiency so we can idealize designs for specific locations.

UCLA Samueli School of Engineering

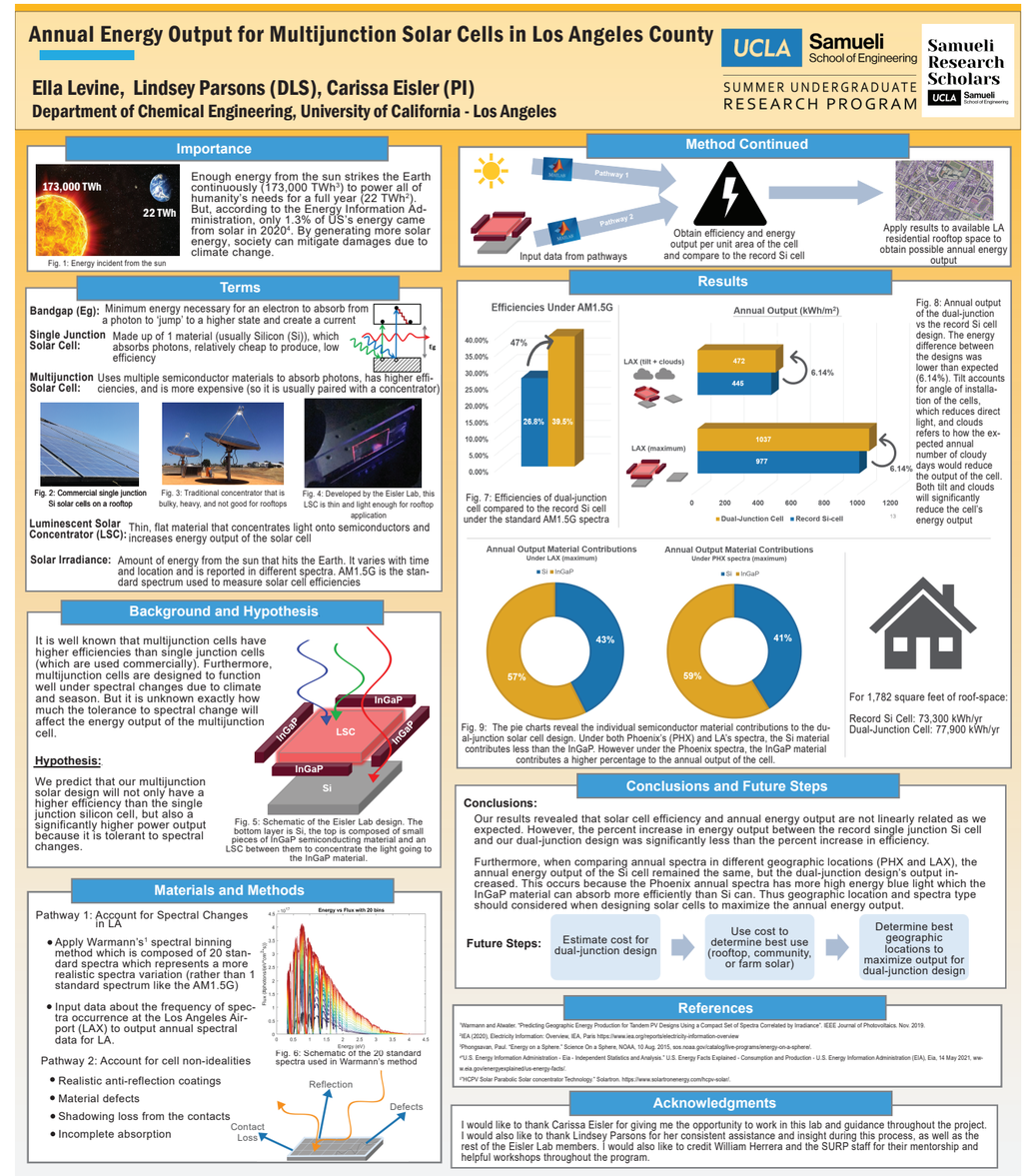

Annual Energy Output for Multijunction Solar Cells in Los Angeles County

Ella Levine, Lindsey Parsons (DLS), Carissa Eisler (PI)
Department of Chemical Engineering, University of California - Los Angeles

UCLA Samueli School of Engineering
SUMMER UNDERGRADUATE RESEARCH PROGRAM
Samueli Research Scholars

Importance

Fig. 1: Energy incident from the sun

Enough energy from the sun strikes the Earth continuously (173,000 TWh[2]) to power all of humanity's needs for a full year (22 TWh[2]). But, according to the Energy Information Administration, only 1.3% of US's energy came from solar in 2020[4]. By generating more solar energy, society can mitigate damages due to climate change.

Terms

Bandgap (Eg): Minimum energy necessary for an electron to absorb from a photon to 'jump' to a higher state and create a current

Single Junction Solar Cell: Made up of 1 material (usually Silicon (Si)), which absorbs photons, relatively cheap to produce, low efficiency

Multijunction Solar Cell: Uses multiple semiconductor materials to absorb photons, has higher efficiencies, and is more expensive (so it is usually paired with a concentrator)

Fig. 2: Commercial single junction Si solar cells on a rooftop

Fig. 3: Traditional concentrator that is bulky, heavy, and not good for rooftops

Fig. 4: Developed by the Eisler Lab, this LSC is thin and light enough for rooftop application

Luminescent Solar Concentrator (LSC): Thin, flat material that concentrates light onto semiconductors and increases energy output of the solar cell

Solar Irradiance: Amount of energy from the sun that hits the Earth. It varies with time and location and is reported in different spectra. AM1.5G is the standard spectrum used to measure solar cell efficiencies

Background and Hypothesis

It is well known that multijunction cells have higher efficiencies than single junction cells (which are used commercially). Furthermore, multijunction cells are designed to function well under spectral changes due to climate and season. But it is unknown exactly how much the tolerance to spectral change will affect the energy output of the multijunction cell.

Hypothesis:

We predict that our multijunction solar design will not only have a higher efficiency than the single junction silicon cell, but also a significantly higher power output because it is tolerant to spectral changes.

Fig. 5: Schematic of the Eisler Lab design. The bottom layer is Si, the top is composed of small pieces of InGaP semiconducting material and an LSC between them to concentrate the light going to the InGaP material.

Materials and Methods

Pathway 1: Account for Spectral Changes in LA

- Apply Warmann's[1] spectral binning method which is composed of 20 standard spectra which represents a more realistic spectra variation (rather than 1 standard spectrum like the AM1.5G)
- Input data about the frequency of spectra occurrence at the Los Angeles Airport (LAX) to output annual spectral data for LA.

Fig. 6: Schematic of the 20 standard spectra used in Warmann's method

Pathway 2: Account for cell non-idealities

- Realistic anti-reflection coatings
- Material defects
- Shadowing loss from the contacts
- Incomplete absorption

Method Continued

Results

Fig. 7: Efficiencies of dual-junction cell compared to the record Si cell under the standard AM1.5G spectra

Fig. 8: Annual output of the dual-junction vs the record Si cell design. The energy difference between the designs was lower than expected (6.14%). Tilt accounts for angle of installation of the cells, which reduces direct light, and clouds refers to how the expected annual number of cloudy days would reduce the output of the cell. Both tilt and clouds will significantly reduce the cell's energy output

Fig. 9: The pie charts reveal the individual semiconductor material contributions to the dual-junction solar cell design. Under both Phoenix's (PHX) and LA's spectra, the Si material contributes less than the InGaP. However under the Phoenix spectra, the InGaP material contributes a higher percentage to the annual output of the cell.

For 1,782 square feet of roof-space:

Record Si Cell: 73,300 kWh/yr
Dual-Junction Cell: 77,900 kWh/yr

Conclusions and Future Steps

Conclusions:

Our results revealed that solar cell efficiency and annual energy output are not linearly related as we expected. However, the percent increase in energy output between the record single junction Si cell and our dual-junction design was significantly less than the percent increase in efficiency.

Furthermore, when comparing annual spectra in different geographic locations (PHX and LAX), the annual energy output of the Si cell remained the same, but the dual-junction design's output increased. This occurs because the Phoenix annual spectra has more high energy blue light which the InGaP material can absorb more efficiently than Si can. Thus geographic location and spectra type should considered when designing solar cells to maximize the annual energy output.

Future Steps: Estimate cost for dual-junction design → Use cost to determine best use (rooftop, community, or farm solar) → Determine best geographic locations to maximize output for dual-junction design

References

[1]Warmann and Atwater. "Predicting Geographic Energy Production for Tandem PV Designs Using a Compact Set of Spectra Correlated by Irradiance". IEEE Journal of Photovoltaics. Nov. 2019.

[2]IEA (2020). Electricity Information: Overview. IEA. Paris https://www.iea.org/reports/electricity-information-overview

[3]Phongsavan, Paul. "Energy on a Sphere." Science On a Sphere, NOAA, 10 Aug. 2015, sos.noaa.gov/catalog/live-programs/energy-on-a-sphere/.

[4]"U.S. Energy Information Administration - Eia - Independent Statistics and Analysis." U.S. Energy Facts Explained - Consumption and Production - U.S. Energy Information Administration (EIA), Eia, 14 May 2021, www.eia.gov/energyexplained/us-energy-facts/.

[5]"HCPV Solar Parabolic Solar concentrator Technology." Solartron. https://www.solartronenergy.com/hcpv-solar/.

Acknowledgments

I would like to thank Carissa Eisler for giving me the opportunity to work in this lab and guidance throughout the project. I would also like to thank Lindsey Parsons for her consistent assistance and insight during this process, as well as the rest of the Eisler Lab members. I would also like to credit William Herrera and the SURP staff for their mentorship and helpful workshops throughout the program.

Angela Liu

Chemical Engineering
Freshman, UCLA

Integrating data-driven and Mechanistic Approaches in Cell Regulatory Pathway Analysis

FACULTY ADVISOR

Aaron Meyer

DAILY LAB SUPERVISOR

Farnaz Mohammadi

DEPARTMENT

Bioengineering

ABSTRACT

Targeted therapies eliminate cancer cells by inhibiting specific dysregulated pathways. While these treatments have proven to extend and save lives, drug resistance is a prevalent issue for currently available drugs. Previous work has identified sets of genes in melanoma that are disproportionately expressed in cancer cells that go on to become resistant after treatment with targeted therapy. However, how these genes form a coordinated pathway is not understood. We used a previously proposed non-linear form of gene regulatory network identification to convert perturbation experiments into an inferred pathway for these genes. Extending this work, we developed an iterative matrix solving method, making this algorithm scalable to many thousands of genes and knockdown conditions, along with allowing us to reason about its statistical properties. We applied this model and then analyzed its results to reveal drivers of melanoma drug resistance development. The matrix was visually represented by a weighted directed diagram, which was analyzed for clustering using the Bellman-Ford distance algorithm for pairs of pre-resistant, resistant, and randomized nodes. In total, this work provides a scalable approach to reasoning about the pathway mechanisms revealed in perturbation experiments.

UCLA Samueli School of Engineering

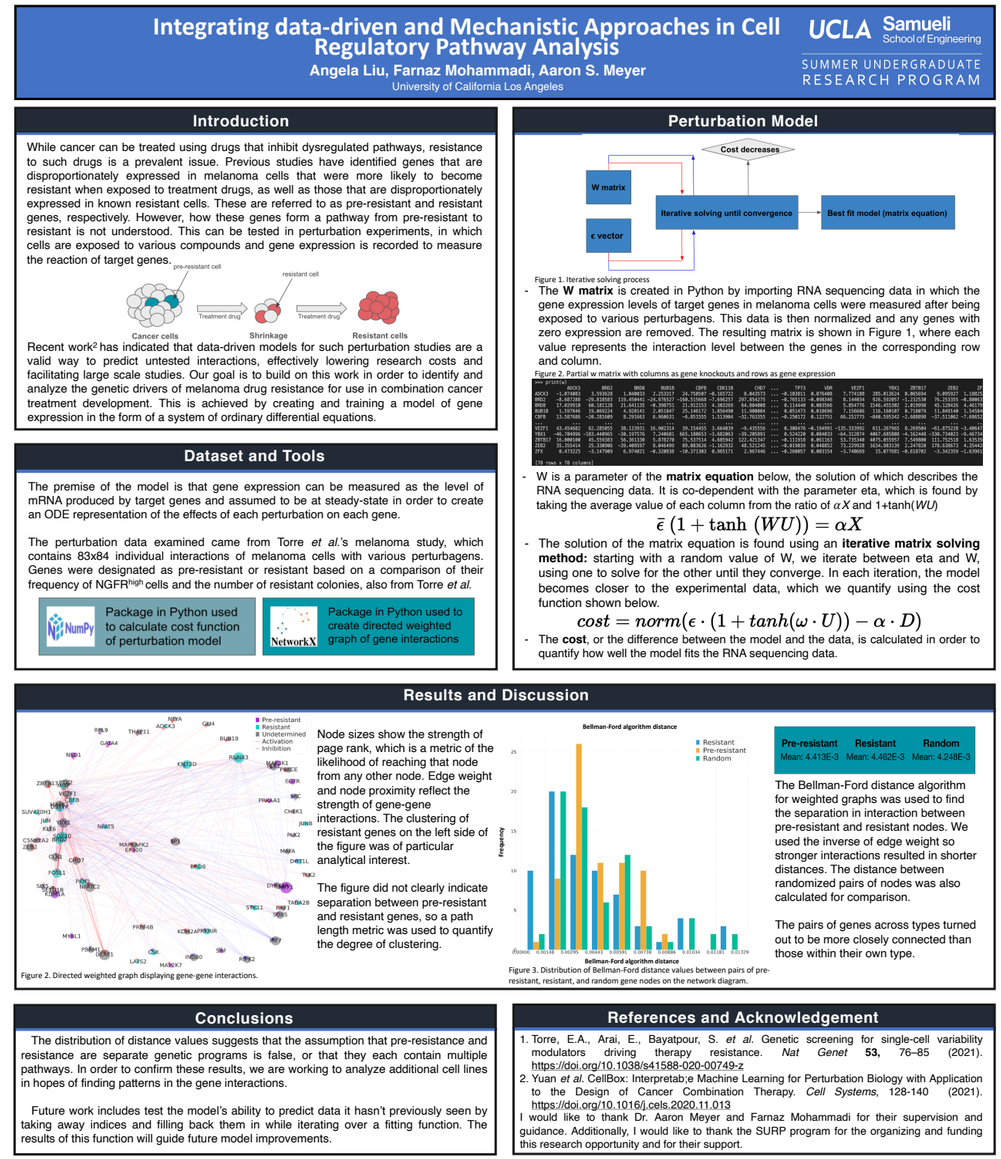

Integrating data-driven and Mechanistic Approaches in Cell Regulatory Pathway Analysis

Angela Liu, Farnaz Mohammadi, Aaron S. Meyer
University of California Los Angeles

UCLA Samueli School of Engineering
SUMMER UNDERGRADUATE RESEARCH PROGRAM

Introduction

While cancer can be treated using drugs that inhibit dysregulated pathways, resistance to such drugs is a prevalent issue. Previous studies have identified genes that are disproportionately expressed in melanoma cells that were more likely to become resistant when exposed to treatment drugs, as well as those that are disproportionately expressed in known resistant cells. These are referred to as pre-resistant and resistant genes, respectively. However, how these genes form a pathway from pre-resistant to resistant is not understood. This can be tested in perturbation experiments, in which cells are exposed to various compounds and gene expression is recorded to measure the reaction of target genes.

Figure 1. Iterative solving process

Recent work[2] has indicated that data-driven models for such perturbation studies are a valid way to predict untested interactions, effectively lowering research costs and facilitating large scale studies. Our goal is to build on this work in order to identify and analyze the genetic drivers of melanoma drug resistance for use in combination cancer treatment development. This is achieved by creating and training a model of gene expression in the form of a system of ordinary differential equations.

Dataset and Tools

The premise of the model is that gene expression can be measured as the level of mRNA produced by target genes and assumed to be at steady-state in order to create an ODE representation of the effects of each perturbation on each gene.

The perturbation data examined came from Torre *et al.*'s melanoma study, which contains 83x84 individual interactions of melanoma cells with various perturbagens. Genes were designated as pre-resistant or resistant based on a comparison of their frequency of NGFR^{high} cells and the number of resistant colonies, also from Torre *et al.*

Package in Python used to calculate cost function of perturbation model

Package in Python used to create directed weighted graph of gene interactions

Perturbation Model

Figure 1. Iterative solving process

- The **W matrix** is created in Python by importing RNA sequencing data in which the gene expression levels of target genes in melanoma cells were measured after being exposed to various perturbagens. This data is then normalized and any genes with zero expression are removed. The resulting matrix is shown in Figure 1, where each value represents the interaction level between the genes in the corresponding row and column.

Figure 2. Partial w matrix with columns as gene knockouts and rows as gene expression

- W is a parameter of the **matrix equation** below, the solution of which describes the RNA sequencing data. It is co-dependent with the parameter eta, which is found by taking the average value of each column from the ratio of αX and 1+tanh(WU)

$$\bar{\epsilon}\,(1+\tanh\,(WU)) = \alpha X$$

- The solution of the matrix equation is found using an **iterative matrix solving method:** starting with a random value of W, we iterate between eta and W, using one to solve for the other until they converge. In each iteration, the model becomes closer to the experimental data, which we quantify using the cost function shown below.

$$cost = norm(\epsilon \cdot (1 + tanh(\omega \cdot U)) - \alpha \cdot D)$$

- The **cost**, or the difference between the model and the data, is calculated in order to quantify how well the model fits the RNA sequencing data.

Results and Discussion

Figure 2. Directed weighted graph displaying gene-gene interactions.

Node sizes show the strength of page rank, which is a metric of the likelihood of reaching that node from any other node. Edge weight and node proximity reflect the strength of gene-gene interactions. The clustering of resistant genes on the left side of the figure was of particular analytical interest.

The figure did not clearly indicate separation between pre-resistant and resistant genes, so a path length metric was used to quantify the degree of clustering.

Figure 3. Distribution of Bellman-Ford distance values between pairs of pre-resistant, resistant, and random gene nodes on the network diagram.

Pre-resistant	Resistant	Random
Mean: 4.413E-3	Mean: 4.462E-3	Mean: 4.248E-3

The Bellman-Ford distance algorithm for weighted graphs was used to find the separation in interaction between pre-resistant and resistant nodes. We used the inverse of edge weight so stronger interactions resulted in shorter distances. The distance between randomized pairs of nodes was also calculated for comparison.

The pairs of genes across types turned out to be more closely connected than those within their own type.

Conclusions

The distribution of distance values suggests that the assumption that pre-resistance and resistance are separate genetic programs is false, or that they each contain multiple pathways. In order to confirm these results, we are working to analyze additional cell lines in hopes of finding patterns in the gene interactions.

Future work includes test the model's ability to predict data it hasn't previously seen by taking away indices and filling back them in while iterating over a fitting function. The results of this function will guide future model improvements.

References and Acknowledgement

1. Torre, E.A., Arai, E., Bayatpour, S. *et al.* Genetic screening for single-cell variability modulators driving therapy resistance. *Nat Genet* **53,** 76–85 (2021). https://doi.org/10.1038/s41588-020-00749-z
2. Yuan *et al.* CellBox: Interpretab;e Machine Learning for Perturbation Biology with Application to the Design of Cancer Combination Therapy. *Cell Systems*, 128-140 (2021). https://doi.org/10.1016/j.cels.2020.11.013

I would like to thank Dr. Aaron Meyer and Farnaz Mohammadi for their supervision and guidance. Additionally, I would like to thank the SURP program for the organizing and funding this research opportunity and for their support.

Matthew Lopez

Civil and Environmental Engineering Freshman, UCLA

The Risk of Liquefaction and Sea Level Rise on California's Coastal Communities

FACULTY ADVISOR

Timu Gallien

DAILY LAB SUPERVISOR

Margit Maple

DEPARTMENT

Civil and Environmental Engineering

ABSTRACT

Liquefaction occurs when a high water content soil loses strength during an earthquake and enters a liquid-like state. Sea level rise will elevate local beach groundwater tables and may substantially increase liquefaction risk along the California coastline. Studies have been conducted in Hawaii and Connecticut to understand the combined risk of liquefaction and sea level rise, however studies for the California coastline are limited, as are the publicly available groundwater well data required to make these risk assessments. This research highlights liquefaction risk within specific sites, how sea level rise affects these risks, and considers the impact at various urbanized coastal California sites. Sunset Beach and Newport Beach serve as case studies. Information such as population, number of buildings, and building type are compiled. Geospatial surface terrain data and tidal elevations are then compiled in ArcGIS to create elevation maps for the sites and used to make a general assessment of potential liquefaction damage. For the Sunset Beach site the areas currently within liquefaction zones include 403 buildings and $849 million in housing while Newport Bay includes 6,934 buildings and $26.6 billion in value. Limited groundwater data suggests that groundwater tables within the sites are at a moderate depth. This, combined with the extent that SLR could temporarily increase groundwater levels at the sites through direct inundation suggests that these coastal communities may become increasingly susceptible to liquefaction. Study results emphasize the severity of liquefaction risks and highlight the need to monitor local beach groundwater tables and potential liquefaction conditions to reduce current and future threats to infrastructure.

UCLA Samueli School of Engineering

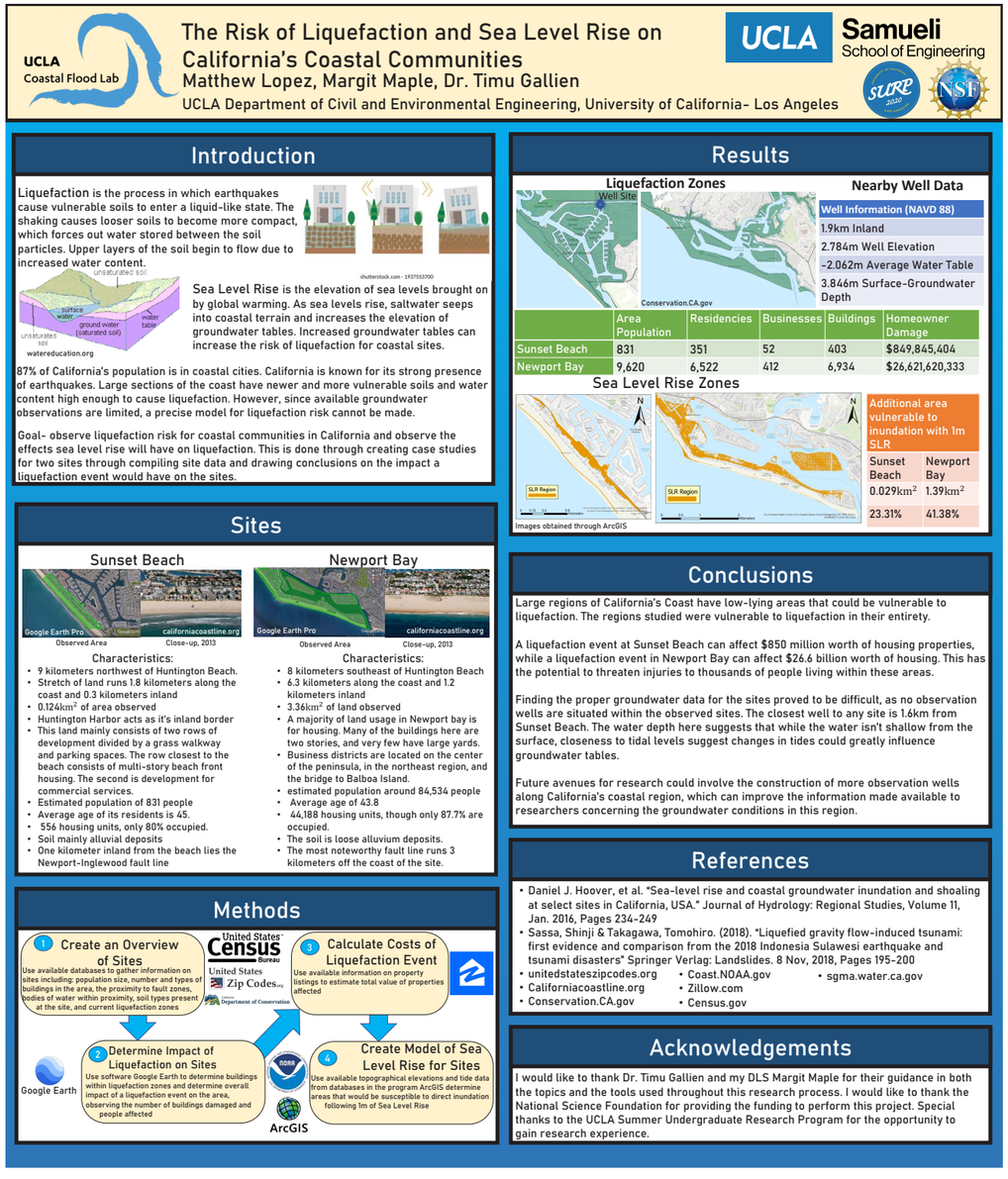

UCLA Coastal Flood Lab

The Risk of Liquefaction and Sea Level Rise on California's Coastal Communities

Matthew Lopez, Margit Maple, Dr. Timu Gallien

UCLA Department of Civil and Environmental Engineering, University of California- Los Angeles

UCLA Samueli School of Engineering

Introduction

Liquefaction is the process in which earthquakes cause vulnerable soils to enter a liquid-like state. The shaking causes looser soils to become more compact, which forces out water stored between the soil particles. Upper layers of the soil begin to flow due to increased water content.

shutterstock.com · 1937553700

unsaturated soil; surface water; ground water (saturated soil); water table; unsaturated soil

watereducation.org

Sea Level Rise is the elevation of sea levels brought on by global warming. As sea levels rise, saltwater seeps into coastal terrain and increases the elevation of groundwater tables. Increased groundwater tables can increase the risk of liquefaction for coastal sites.

87% of California's population is in coastal cities. California is known for its strong presence of earthquakes. Large sections of the coast have newer and more vulnerable soils and water content high enough to cause liquefaction. However, since available groundwater observations are limited, a precise model for liquefaction risk cannot be made.

Goal- observe liquefaction risk for coastal communities in California and observe the effects sea level rise will have on liquefaction. This is done through creating case studies for two sites through compiling site data and drawing conclusions on the impact a liquefaction event would have on the sites.

Sites

Sunset Beach

Google Earth Pro · californiacoastline.org

Observed Area · Close-up, 2013

Characteristics:

- 9 kilometers northwest of Huntington Beach.
- Stretch of land runs 1.8 kilometers along the coast and 0.3 kilometers inland
- 0.124km^2 of area observed
- Huntington Harbor acts as it's inland border
- This land mainly consists of two rows of development divided by a grass walkway and parking spaces. The row closest to the beach consists of multi-story beach front housing. The second is development for commercial services.
- Estimated population of 831 people
- Average age of its residents is 45.
- 556 housing units, only 80% occupied.
- Soil mainly alluvial deposits
- One kilometer inland from the beach lies the Newport-Inglewood fault line

Newport Bay

Google Earth Pro · californiacoastline.org

Observed Area · Close-up, 2013

Characteristics:

- 8 kilometers southeast of Huntington Beach
- 6.3 kilometers along the coast and 1.2 kilometers inland
- 3.36km^2 of land observed
- A majority of land usage in Newport bay is for housing. Many of the buildings here are two stories, and very few have large yards.
- Business districts are located on the center of the peninsula, in the northeast region, and the bridge to Balboa Island.
- estimated population around 84,534 people
- Average age of 43.8
- 44,188 housing units, though only 87.7% are occupied.
- The soil is loose alluvium deposits.
- The most noteworthy fault line runs 3 kilometers off the coast of the site.

Methods

1. **Create an Overview of Sites** — Use available databases to gather information on sites including: population size, number and types of buildings in the area, the proximity to fault zones, bodies of water within proximity, soil types present at the site, and current liquefaction zones
2. **Determine Impact of Liquefaction on Sites** — Use software Google Earth to determine buildings within liquefaction zones and determine overall impact of a liquefaction event on the area, observing the number of buildings damaged and people affected
3. **Calculate Costs of Liquefaction Event** — Use available information on property listings to estimate total value of properties affected
4. **Create Model of Sea Level Rise for Sites** — Use available topographical elevations and tide data from databases in the program ArcGIS determine areas that would be susceptible to direct inundation following 1m of Sea Level Rise

United States Census Bureau · United States Zip Codes.org · Department of Conservation · Google Earth · NOAA · ArcGIS

Results

Liquefaction Zones

Well Site · Conservation.CA.gov

Nearby Well Data

Well Information (NAVD 88)
1.9km Inland
2.784m Well Elevation
-2.062m Average Water Table
3.846m Surface-Groundwater Depth

	Area Population	Residencies	Businesses	Buildings	Homeowner Damage
Sunset Beach	831	351	52	403	$849,845,404
Newport Bay	9,620	6,522	412	6,934	$26,621,620,333

Sea Level Rise Zones

SLR Region

Additional area vulnerable to inundation with 1m SLR	
Sunset Beach	Newport Bay
0.029km^2	1.39km^2
23.31%	41.38%

Images obtained through ArcGIS

Conclusions

Large regions of California's Coast have low-lying areas that could be vulnerable to liquefaction. The regions studied were vulnerable to liquefaction in their entirety.

A liquefaction event at Sunset Beach can affect $850 million worth of housing properties, while a liquefaction event in Newport Bay can affect $26.6 billion worth of housing. This has the potential to threaten injuries to thousands of people living within these areas.

Finding the proper groundwater data for the sites proved to be difficult, as no observation wells are situated within the observed sites. The closest well to any site is 1.6km from Sunset Beach. The water depth here suggests that while the water isn't shallow from the surface, closeness to tidal levels suggest changes in tides could greatly influence groundwater tables.

Future avenues for research could involve the construction of more observation wells along California's coastal region, which can improve the information made available to researchers concerning the groundwater conditions in this region.

References

- Daniel J. Hoover, et al. "Sea-level rise and coastal groundwater inundation and shoaling at select sites in California, USA." Journal of Hydrology: Regional Studies, Volume 11, Jan. 2016, Pages 234-249
- Sassa, Shinji & Takagawa, Tomohiro. (2018). "Liquefied gravity flow-induced tsunami: first evidence and comparison from the 2018 Indonesia Sulawesi earthquake and tsunami disasters" Springer Verlag: Landslides. 8 Nov, 2018, Pages 195-200
- unitedstateszipcodes.org
- Californiacoastline.org
- Conservation.CA.gov
- Coast.NOAA.gov
- Zillow.com
- Census.gov
- sgma.water.ca.gov

Acknowledgements

I would like to thank Dr. Timu Gallien and my DLS Margit Maple for their guidance in both the topics and the tools used throughout this research process. I would like to thank the National Science Foundation for providing the funding to perform this project. Special thanks to the UCLA Summer Undergraduate Research Program for the opportunity to gain research experience.

Quinlan McKnight

Civil Engineering
Sophomore, UCLA

Presence of Microplastics in Stormwater Wetlands Delays Microbial Methane Production

FACULTY ADVISOR

Sanjay Mohanty

DAILY LAB SUPERVISOR

Renan Valenca

DEPARTMENT

Civil and Environmental Engineering

ABSTRACT

Wetland environments are home to biological processes that emit methane - a greenhouse gas that accelerates climate change. Methanogens, methane-producing bacteria, are commonly present in these wetlands that receive stormwater runoff containing a range of contaminants including microplastics (MPs). MPs are known to suppress microbial activity, but their effect on the methanogenesis process and on the diversity of microbial communities in wetland environments remains unknown. To identify the impact of MPs on the methane production from wetland sediments, we performed a series of laboratorial batch experiments where different wetland sediment sizes were exposed to MPs under aerobic and anaerobic conditions while monitoring the production of methane. The batch experiments were kept in incubators at optimum conditions for methane production. Our results show that, under aerobic conditions, large sediments (> 2.0 mm) produced 100 times more methane than fine sediments (< 2.0 mm), possibly due to the decomposition of organic matter present only within large sediments. Under anaerobic conditions, fine particles increased their production by more than 40 times when acetate was present in solution, proving that wetland sediments have the capacity for methane production when nutrients are available. The presence of MPs among fine sediments with acetate caused a delay and suppressed methane production, possibly due to the direct interaction between MPs and methanogens, as well as the indirect interaction between MPs and acetate, as both processes could suppress methane production. Overall, the results furnish the understanding of methane fluxes in relation to microplastic transport in wetland environments.

UCLA Samueli School of Engineering

Presence of Microplastics in Stormwater Wetlands Delays Microbial Methane Production

Samueli Research Scholars
UCLA Samueli School of Engineering

Quinlan McKnight, Renan Valença, Dr. Sanjay K. Mohanty
Department of Civil and Environmental Engineering – University of California, Los Angeles

UCLA Samueli School of Engineering
SUMMER UNDERGRADUATE RESEARCH PROGRAM

Introduction

Images: Flaticon.com

Wetlands (WLs) are biologically diverse environments; however, methanogens (methane-producing bacteria) there are the main source of methane emissions into the atmosphere, a climate change accelerator.

WLs receive stormwater runoff that contain emerging contaminants such as microplastics (MPs). It is known MPs suppress microbial activity, but the effect of MPs on wetland methane production is unknown.

What is the effect of MPs on methane production and microbial communities in wetlands?

Materials and Methods

WL sediments were collected from the Ballona Wetlands in Los Angeles, CA. On the same day as collection, sediments were sieved to separate the fine sediments (< 2.0 mm) from large (> 2.0 mm) and used in the following experiments:

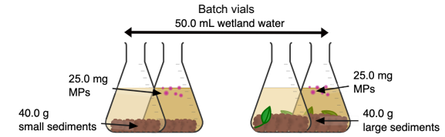

Fig. 1: Experiment 1 -- Control and MP batch vials containing small or large sediments under aerobic conditions. Vials were kept in an incubator at optimum conditions; gas samples were extracted in the same manner as **Fig. 2** to measure methane concentration.

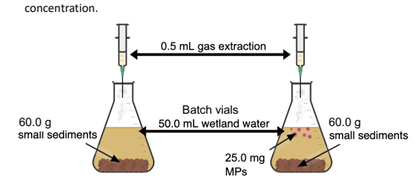

Fig. 2: Experiment 2 – Control and MP batch vials containing fine sediments and nutrients (acetate) under anaerobic conditions as achieved by **Fig. 3**. Vials were kept in an incubator at optimum conditions; gas samples were extracted periodically and analyzed using gas chromatography.

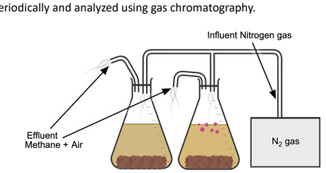

Fig. 3: Nitrogen gas purged into batch vials to achieve anaerobic conditions.

Results

Fig. 4: Experiment 1 –

Large sediments produced significantly more methane ($p < 0.05$) than fine sediments under aerobic conditions in both the control and MP batch vials.

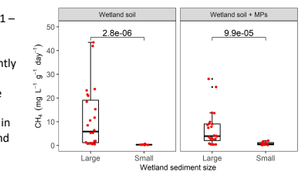

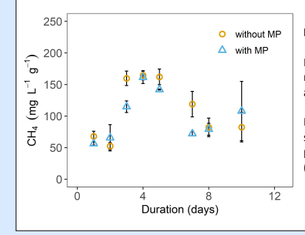

Fig. 5: Experiment 2 --

Fine sediments produced more methane when acetate was present.

MPs delayed and suppressed the production of methane (day 2 – day 8).

Conclusions

In Experiment 1, the decay of organic matter only present among large sediments may have caused the magnitude difference of methane production. For this reason, future experiments will only utilize small sediments, as the research focus is on microbial production of methane.

In Experiment 2, results suggest that fine sediments have the capacity to produce methane when nutrients are available. MPs delayed and suppressed methane production, possibly due to the direct interaction between MPs and methanogens, and/or between MPs and acetate.

Future Work

Microbial DNA analysis will be performed on the sediments to connect the varying methane concentrations with bacterial health.

Since rising global temperatures cause wildfire frequency to increase, Experiment 2 will be recreated with wildfire residues to understand the effect of these contaminants on methane production.

Acknowledgements

Thank you to my Daily Lab Supervisor, Renan Valença, and my faculty advisor, Dr. Sanjay Mohanty, for the invaluable support I have received. Thank you to the Summer Undergraduate Research Program, the Samueli Research Scholars Program, and the Samueli Foundation for this research opportunity.

Krisha Minocha

Computer Engineering
Freshman, UCLA

Camera-based Heart Rate Estimation Focused on Mitigating Bias

FACULTY ADVISOR

Achuta Kadambi

DAILY LAB SUPERVISOR

Pradyumna Chari

DEPARTMENT

Electrical and Computer Engineering

ABSTRACT

The COVID-19 pandemic has led to an influx of telehealth appointments, causing difficulty in assessing vital signs virtually. Our work focuses on remote photoplethysmography (R-PPG), the concept of measuring heart rate using color fluctuations in the face. Many different algorithms already exist with varying levels of success; however, one major gap is the lack of performance of these existing algorithms on darker skin tones, which, given the prevalence of cardiovascular disease in African American communities, creates a pressing issue. We have employed a VGG-style convolutional network known as DeepPhys to learn different spatial masks and increase robustness across the board. My work has focused on improving this existing network to increase medical accuracy by manipulating the structure of the network along with training parameters.

UCLA Samueli School of Engineering

Camera-based Heart Rate Estimation Focused on Mitigating Bias

Krisha Minocha, Pradyumna Chari, Professor Achuta Kadambi
Department of Electrical and Computer Engineering - UCLA

Introduction

There has recently been a notable influx in telehealth visits due to the COVID-19 pandemic. While telehealth has created a way to provide patient care remotely, it is extremely difficult to assess vital signs such as heart rate, breathing rate, etc., indicating that there is clearly a need for contactless heart rate sensing solutions. While there are existing computer vision solutions available, they exhibit a bias against darker skin tones.

Key Concepts

Remote Photoplethysmography (R-PPG)
- Type of algorithm focused on using subtle color variations in the face to measure a blood volume pulse and, consequently, estimate heart rate.

Convolutional Neural Network
- A computer system modeled on the human brain and nervous system, specifically focused on mimicking the optic nerve and image processing

Objective

I aim to implement an improved computer vision model for measuring heart rate using deep learning. My goal is to increase performance specifically on darker skin tones.

VITAL Dataset

Vital-sign Imaging for Telemedicine AppLications developed by Visual Machines Group at UCLA
- At least 432 videos of 54 subjects
- Focus on a diverse dataset in terms of gender, race, age, skin tone, etc.
- Using two different camera angles and four different lighting conditions with only a smartphone camera

I will be working to train the algorithm on this dataset in order to ensure optimal performance across the board.

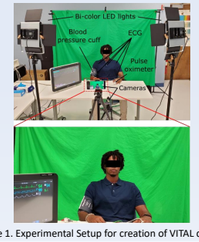

Figure 1. Experimental Setup for creation of VITAL dataset

Proposed Algorithm

My proposed algorithm will build of off the existing DeepPhys algorithm developed by W. Chen and D. McDuff consisting of:
- A VGG-Style Convolutional Neural Network (up to 19 layers)
- Learns spatial masks for regions of interest to maximize performance and robustness
- Emphasis on diffuse component, ignoring the mirror-like reflections of the skin
- Uses two streams: Motion and Appearance in order to maximize performance

This algorithm was able to improve performance with motion and talking. However, there is still a bias in terms of skin tone. My proposed changes will be to the structure of the model to hopefully improve performance across the board. I plan on doing this by using different activation and loss functions and observing the results.

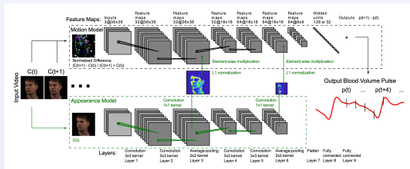

Figure 2. Proposed Algorithm Structure Using Both Appearance and Motion Streams to Increase Robustness

Conclusion and Results

Activation/Loss Function Combination	Mean Absolute Error (bpm)
rrelu/softmarginloss	18
tanh/MSE	13.166
selu/pearson	12.73
relu/MSE	12.57
relu/L!Loss	12.57
rrelu/MSE	11.257
rrelu/L1Loss	11.257
rrelu/pearson	11.251

Table 1. Table of experimental results of loss/activation function manipulation

This work furthers previous algorithmic advances such as the existing DeepPhys algorithm to increase accuracy. We can see that regardless of loss function, the rrelu activation function creates the best results. However, there is still a large margin of error, which needs to be corrected. This work can also be extended outside of the medical realm into reducing bias in other computer vision applications such as facial recognition, etc.

References

1. Chari, Pradyumna, et al. "Diverse R-PPG: Camera-Based Heart Rate Estimation for Diverse Subject Skin-Tones and Scenes." *ArXiv*, 2020. https://arxiv.org/pdf/2010.12769.pdf
2. Chen, Weixuan, and Daniel McDuff. "DeepPhys: Video-Based Physiological Measurement Using Convolutional Attention Networks." *ArXiv*, 2018, https://arxiv.org/pdf/1805.07888.pdf

Acknowledgements

We would like to thank the UCLA Summer Undergraduate Research Program for organizing this research internship and the Samueli Research Scholars Program for funding it. We would also like to thank the UCLA Fast Track to Success Electrical and Computer Engineering Program for their continued guidance and support. I would also like to thank Pradyumna and Professor Kadambi for challenging me and creating such a supportive and creative atmosphere for learning.

Zofia Orlowski

Mechanical Engineering
Sophomore, UCLA

Internet of Things (IoT) Technology for Electrowetting-on-dielectric (EWOD) Devices

FACULTY ADVISOR

Chang-Jin Kim

DAILY LAB SUPERVISOR

Qining Wang

DEPARTMENT

Aerospace and Mechanical Engineering

ABSTRACT

Electrowetting-on-dielectric (EWOD) is a mechanism that enables the manipulation of droplets through electrical signals alone. Due to its advantages for droplet-based microfluidics, such as the simplicity in both device design and fabrication, EWOD has demonstrated its utility in numerous biochemical and biomedical applications, especially lab-on-a-chip. However, currently the EWOD technology is being utilized by only a small number of labs who have proper engineering backgrounds, enough resources to design and fabricate devices to fulfill their goals, and control systems and software to operate the devices. To combat this barrier, the UCLA Micro and Nano Manufacturing Laboratory is developing a cloud-based cyber-manufacturing platform for common users to gain easy access to the EWOD technology. In furthering the mission, the lab is exploring a remote operation of the EWOD control system by introducing an Internet of Things (IoT)-based intermediate system. This remote operation will serve as a gateway to an envisioned lab-on-cloud that will help democratize EWOD technology. Acting as a broker for information exchange between a backend server and EWOD control system, the intermediate system is designed to run users' instruction files, communicate its messages to the EWOD control system, and operate alongside a camera for users to remotely monitor their experiments. My work has involved developing a proof-of-concept demonstration that one can operate an EWOD control system by sending the necessary commands from a remote location.

UCLA Samueli School of Engineering

Samueli Research Scholars

Internet of Things (IoT) Technology for Electrowetting-on-dielectric (EWOD) Devices

Zofia Orlowski, Qining "Leo" Wang, Dr. Chang-Jin "CJ" Kim
Department of Mechanical Engineering, University of California, Los Angeles

UCLA Samueli School of Engineering
SUMMER UNDERGRADUATE RESEARCH PROGRAM

Introduction and Background

In digital microfluidics, **electrowetting-on-dielectric** (**EWOD**) is a mechanism that permits the manipulation of droplets through electrical signals alone. EWOD has several biochemical and biomedical applications due to its advantages, such as its simplicity in device design and fabrication. A principal EWOD application is **lab-on-a-chip**. Typical lab-on-a-chip advantages include lower fluid volume consumptions and faster response times for experiments.

However, EWOD technology is only being used by a small number of labs who possess: proper engineering backgrounds, enough resources to design and fabricate EWOD devices, and the proper control systems and software to operate these devices. To help democratize the technology, the UCLA Micro and Nano Manufacturing Laboratory is developing a cloud-based, **EWOD cybermanufacturing platform** where users' can translate their design ideas into manufactured digital microfluidic devices.

My role in the project involved integrating **Internet of Things** (**IoT**) technology (where experiments are driven through issuing commands over the internet) to enable remote access to the lab's EWOD control systems. IoT access will serve as a gateway to an envisioned lab-on-cloud. Furthermore, in the future it can help onboard new users to the platform who prefer to obtain EWOD devices upfront.

Figure 1. Science of EWOD: A beaded droplet on a repellent surface can become wetted when voltage is applied. This mechanism is used for droplet manipulation.

Figure 2. Example of a common (not EWOD) microfluidic chip used to perform lab-on-a-chip research

Figure 3. Image of EWOD device in EWOD control system and operated via graphic user interface (GUI) developed in Prof. CJ Kim's lab.

Results

We were able to begin a proof-of-concept demonstration that one can operate an EWOD control system by sending commands from a remote location.

The mock experimental setup consisted of a USB **webcam**, Raspberry Pi, and mock EWOD control system. We used **Motion**, a software package which is designed to monitor cameras and security devices, with the Raspberry Pi to network a video stream via **HTTP.** We tested to see how the camera would pick up on droplets and their movement and verified that we can transmit video through the Raspberry Pi.

We also created test code to send commands regarding droplet movement, such as left, right, up, down, or split over AWS. AWS IoT has a **MQTT test client** where we were able to test sending messages regarding droplet manipulation between different endpoints.

Figure 6. Image of mock EWOD control system and camera experimental setup for remote droplet viewing.

Figure 7. Code to operate Motion with the Raspberry Pi. Code using FFmpeg to convert video stream to a format that can be sent over RTMPS to the backend.

Figure 8. Sending messages between the Amazon IoT MQTT test client and our test code.

Figure 9. Example of test code written to send commands regarding droplet splitting.

Materials and Methods

Materials needed for the IoT project are: the EWOD control system, a Raspberry Pi (microcomputer), and a USB webcam (imaging module).

Proposed **system architecture** (designed by Leo Wang and Brian Cheng, Figure 4): The EWOD control system communicates with the Raspberry Pi through a USB connection. The Raspberry Pi acts as an intermediate deviceor broker for information exchange between the EWOD control system and server hosting the backend and GUI. Desired internet devices are further connected to this server.

Figure 4. Overall architecture illustrating inter-process communication for the system (designed by Leo Wang and Brian Cheng).

Proposed **Raspberry Pi architecture** (designed by Leo Wang and Brian Cheng, Figure 5): An intermediate device is needed for IoT applications since it has a static IP address. The Raspberry Pi was chosen as our intermediate device since it already has a USB port, and it can simultaneously run multiple programs and processes. The Raspberry Pi is programmed to carry out various tasks, including sending and receiving information between the backend and EWOD control system, sending information to Amazon Web Services (AWS) for IoT, parsing EWOD files (instructions for droplet actuation), and operating with a USB webcam.

Figure 5. Raspberry Pi architecture exhibiting device's functions (designed by Leo Wang and Brian Cheng).

Conclusions and Future Work

Overall, we began a proof-of-concept demonstration for remote operation of an EWOD control system by testing USB camera integration with the Raspberry Pi and the capabilities of AWS IoT. The full proof-of-concept code is still in the process of being tested with the Raspberry Pi and the EWOD control system in the lab. **Future work** will expand on the proof-of-concept and involve more functionalities, such as parsing an EWOD instructions file. Moreover, a one-to-many design for the system will be implemented, such that one Raspberry Pi may control multiple EWOD control systems.

References

[1] X. Huang, C. -C. Liang, J. Li, T. -Y. Ho and C. -J. Kim, "Open-Source Incubation Ecosystem for Digital Microfluidics — Status and Roadmap: Invited Paper," 2019 IEEE/ACM International Conference on Computer-Aided Design (ICCAD), 2019, pp. 1-6, doi: 10.1109/ICCAD45719.2019.8942172.
[2] J. Li, S. Chen, and C.-J. Kim, "Low-Cost and Low-Topography Fabrication of Multilayer Interconnections for Microfluidic Devices", Journal of Micromechanics and Microengineering, Vol. 30, No. 7, May 2020, 077001.
[3] https://stock.adobe.com/search?k=micro%20fluidic&search_type=longtail-carousel-view-results

Acknowledgements

I would like to thank Dr. CJ Kim, Leo Wang, and Brian Cheng at the Micro and Nano Manufacturing Laboratory for sharing their work and guiding me through this project. I extend further thanks to the National Science Foundation for funding this project (Award No. 1720499) and UCLA'S Summer Undergraduate Research Program.

Samantha Rafter

Electrical Engineering
Freshman, UCLA

Optimization of Double Ridge Metasurface for Quantum Cascade External Cavity Laser

FACULTY ADVISOR

Benjamin Williams

DAILY LAB SUPERVISOR

Eilam Morag

DEPARTMENT

Electrical and Computer Engineering

ABSTRACT

Terahertz light has demonstrated the ability to identify complex molecules via spectroscopy. However, its potential to do so has been largely untapped due to a lack of capable, broadband, non-dispersive sources. The double ridge design of the metasurface is a viable path toward bridging this gap by broadening the amplification bandwidth of metasurfaces, which may then be used to create widely tunable quantum cascade external-cavity lasers with low group delay dispersion (GDD). The design consists of repeating units of two differently sized ridges, each of which corresponds to a resonant frequency, at which there is a peak in reflectance (a measure of the amplification of light). Altering the widths of the ridges and the separation between them allows for manipulation of the resonant frequencies so that they are near each other, creating a continuous range of frequencies where amplification is high. Previously, the ridge widths and separation of the ridges were determined by running simulations where tested dimensions were manually decided by the user, who would then analyze the collected data to determine favorable geometries. To more efficiently and accurately find a geometry that could be considered optimal, MATLAB functions representing broadband reflectance and GDD were written in order to quantify the values to be optimized. The simulation software COMSOL Multiphysics as well as its associated optimization module were then used with these functions to create and run optimization studies that determined the geometry of the ridges that minimized dispersion while maintaining broadband reflectance. Initial results suggest that GDD could be improved upon by 1.72% while maintaining the same broadband performance as a previous design, and could be improved upon by 7.48% at a slight cost (0.125 THz) to the bandwidth.

UCLA Samueli School of Engineering

Optimization of Double Ridge Metasurface for Quantum Cascade External Cavity Laser

Samantha Rafter, Eilam Morag, and Professor Benjamin Williams
Department of Electrical and Computer Engineering, University of California, Los Angeles

Samueli Research Scholars
UCLA Samueli School of Engineering
SUMMER UNDERGRADUATE RESEARCH PROGRAM

Introduction & Background

Key Terms

- **Reflectance:** Ratio of Power Out : Power In
- **Dispersion:** Separation of light based on frequency/wavelength; typically undesirable in optics

Previous Research

- **Double Ridge Metasurface:** Amplifying reflector
  - Composed of repeating units of 2 differently sized ridges, the widths of which determine the locations of resonant frequencies
  - Viable design for pairing with output coupler (***Fig. 1(a)***) to achieve a widely tunable Vertical External Cavity Surface Emitting Laser (**VECSEL**) with low dispersion

Fig. 1

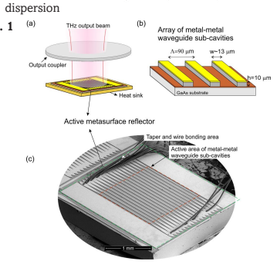

Fig. 1 ***(a)*** *Shows the structure of a VECSEL* ***(b)*** *Shows the composition of a metasurface, while* ***(c)*** *shows its structure*

Objective

Gaps in Knowledge

- Previously, broadband designs were found by running simulations using user-defined inputs for the ridge widths, then analyzing collected data to find optimal geometries with broad ranges of high reflectance.
- *However,* this process is time consuming and imprecise, since geometries between step sizes are not tested.

→ ***There is significant room for improvement in finding a more accurate, optimized geometry for a metasurface with broad amplification***

Fig. 2

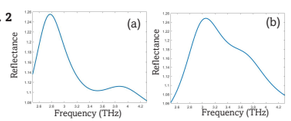

Fig. 2 ***(a)*** *Shows the two resonant frequencies of a double ridge metasurface* ***(b)*** *Shows a user optimized design where ridge widths were altered in order to bring the peak frequencies nearer to each other, creating a broad range over which there is high reflectance*

Objective

Utilize simulation software to automatically find an optimized geometry of the double ridge design that minimizes dispersion while maintaining broadband reflectance.

Materials

COMSOL Multiphysics
COMSOL Optimization Module
MATLAB

Methods

1. **Study relationships** between parameters and figures of merit by running simulations with varying ridge widths and spacing to better understand effects of changing the geometry, and to find a good starting point for optimizing.
2. **Create optimization infrastructure** within COMSOL. Begin by creating MATLAB functions to quantify GDD and broadband reflectance. Set ridge widths and spacing as control variables and set the study to minimize the GDD MATLAB function. Decide and set a constraint so that the solution must meet a certain broadband reflectance requirement.
3. **Collect and analyze data.** Run the optimization study using viable algorithms and improve parameters/constraint/starting point as necessary. Conduct further testing of promising geometries.

Results - Qualitative

General optimization infrastructure was created, and insights into the workings of the optimization module were gained.

COMSOL begins by collecting data for every frequency step (**1**), then exports this data to the MATLAB functions (**2**). These functions return values to COMSOL (**3**), which then analyzes the data and alters the control variables in an attempt to improve the objective.

Fig. 3

Fig. 3 shows a scatterplot of data returned from an optimization study in which GDD was minimized. Data points become denser (red box) as the solver gets closer to finding a solution.

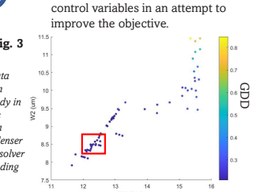

Results - Quantitative

Fig. 4

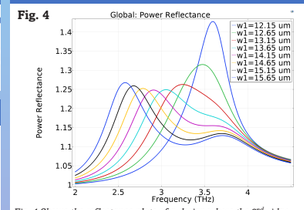

Fig. 4 Shows the reflectance plots of a design where the 2nd ridge width is fixed at 9.45 um, while the 1st ridge width is altered. As the 1st ridge gets wider, its resonant frequency moves to the right. The starting point for optimization was chosen to be a design with even spacing, where ridge 1 = 13.65 um and ridge 2 = 9.45 um (See step 1 of methods).

Fig. 5

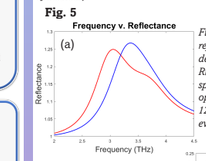

Fig. 5 ***(a)*** *Shows the reflectance plots of the baseline design (Ridge 1: 13.65 um, Ridge 2: 9.45 um, even spacing) in red, and a design optimized for GDD (Ridge 1: 12.69 um, Ridge 2: 9.13 um, even spacing) in blue.*

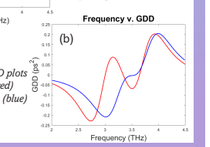

Fig. 5 ***(b)*** *Shows the GDD plots For the baseline design (red) and the optimized design (blue)*

Conclusions

A design optimized for GDD was found that improved the maximum, absolute value of GDD from the baseline design by 8.89% (Fig. 5 (b)). This design maintains a relatively wide bandwidth that is 0.2 THz narrower than the baseline, decreasing its bandwidth by 16.26% (Fig 5 (a)). More generally, it was found that the optimization module of COMSOL is capable of finding improved double ridge geometries.

Future Directions

Further investigation of design optimization can be done, especially with regards to altering the spacing between ridges. The optimization module can also be used to attempt to optimize other pre-existing metasurface designs.

References

Curwen, C., Reno, J. and Williams, B. (2020), Broadband metasurface design for terahertz quantum-cascade VECSEL. Electron. Lett., 56: 1264-1267. https://doi.org/10.1049/el.2020.1963

Acknowledgements

I would like to thank Professor Williams for the opportunity to work in his lab this summer, as well as Eilam Morag for his support on the project. Special thanks to Women in Engineering at UCLA for funding the project through the Samueli Research Scholars program.

Dolores Rodriguez

Chemical Engineering
Junior, UCLA

The Effects of Mass Transfer on CO2 Reduction

FACULTY ADVISOR

Carlos G. Morales-Guio

DAILY LAB SUPERVISOR

Joonbaek Jang

DEPARTMENT

Chemical Engineering

ABSTRACT

Carbon dioxide is the most abundant greenhouse gas in the atmosphere emitted through human activities. However, through an electrochemical process CO2 can be converted into more useful products such as fuels and feedstock chemicals. To improve this process so that selectivity is increased towards these more desirable products, this study will explore how mass transport affects the product distribution of the electroreduction of CO2. We alter the mass transportation of CO2 to the catalytic surface by rotating the catalyst. A cylindrical Cu catalyst is used and rotation speeds of 200 and 400 rpm are tested. The applied potential is also varied from -1.31 V vs SHE to -1.67 V vs SHE. This study provides new insights into what may be the optimal rotation speed that will produce the highest selectivity towards more desirable products, in turn opening up the possibility of CO2 reduction being a new avenue of renewable energy.

UCLA Samueli School of Engineering

The Effects of Mass Transfer on CO_2 Reduction

By Dolores Rodriguez with Joonbaek Jang and Dr. Carlos G. Morales-Guio
Laboratory of Electrochemical Systems Engineering
Department of Chemical Engineering, University of California, Los Angeles

Samueli Research Scholars

UCLA Samueli School of Engineering
SUMMER UNDERGRADUATE RESEARCH PROGRAM

Introduction

CO_2 is the most abundant greenhouse gas in the atmosphere emitted through human activities. This study contributes to the ongoing research on how to reduce CO_2 into fuel and feedstock chemicals in a carbon neutral process. The reduction of CO_2 could prove to be a very useful and new avenue of renewable energy.

Objective

The objective of this study is to explore how mass transport affects the product distribution of the electrochemical reduction of carbon dioxide. More specifically, we will be looking into how rotating the catalyst, and in doing so, changing the mass transfer of carbon dioxide to the catalyst surface affects the product distribution.

Principles

Current Density

- Current density which is the density of electrons flowing from the catalyst
- This is how we measure the activity of a catalyst
- The more active a catalyst is, the more electrons that will be transferred, and therefore a higher current density

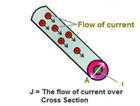

Figure 1[1]: Flow of current through a cross-sectional area

Mass Transfer

- Mass transfer is the net movement of mass from one location to another
- We will be looking at the mass transfer of CO_2 to the catalyst surface.

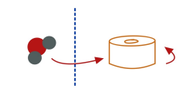

Figure 2: Carbon dioxide molecule traveling to a rotating catalyst

Materials

The electroreduction of carbon dioxide occurs in a custom rotation cell.

The programs Peaksimple [2] and Bruker Topspin [3] are used to identify and quantify the resulting products.

Methods

1. Prepare the Catalyst Surface

The catalyst is first mechanically polished and then electropolished.

2. Running the experiment

The catalyst is placed in the cell where it rotates. The rotation speeds and potentials applied to the system are varied.

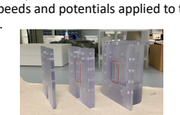

Figure 3: The custom rotation cell

3. Product Quantification

After the experiment is finished, the liquid products are analyzed using Bruker Topspin while the gas products are analyzed using Peaksimple.

Results

Partial Current Density vs Potential at 200 rpm

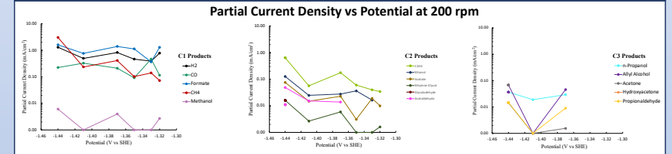

Figure 4: Partial Current Densities of Gas Products vs Potential at 200 rpm. Plots are separated into C1, C2, and C3 products.

Partial Current Density vs Potential at 400 rpm

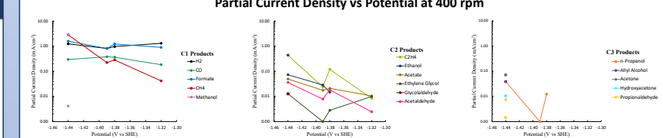

Figure 7: Partial Current Densities of Gas Products vs Potential at 400 rpm. Plots are separated into C1, C2, and C3 products.

Conclusions

Our results don't show a great difference in the range of partial current densities of each product between the two rotation speeds. However, there are noticeable differences in the onset potential of each product between the two rotation speeds. The onset potential is the lowest overpotential at which the product is detected. At 400 rpm, most C3 products have a higher onset potential than at 200 rpm.

For future experiments, data should be collected at more potentials to better depict and define what the partial current density looks like at each rotation speed.

References

[1] Current Density, https://byjus.com/physics/current-density/

[2] Peaksimple Logo, https://www.sri-instruments-europe.com/en/products/software/peak-simple.php

[3] Bruker Topspin Logo, https://nmr.wp.st-andrews.ac.uk/bruker-topspin/

Acknowledgements

I would like to thank to my P.I., Dr. Carlos G. Morales-Guio and my daily lab supervisor, Joonbaek Jang for their guidance and mentorship. I would like to thank William Herrera and the rest of the SURP program administrators for their resources. I would also like to thank Samueli Research Scholars for funding this research.

Lizeth Vera

Computer Science
Freshman, UCLA

Development of SpectraPlot Application for Broadband Spectral Line Survey

FACULTY ADVISOR

R. Mitchell Spearrin

DAILY LAB SUPERVISOR

Chuyu Wei

DEPARTMENT

Aerospace and Mechanical Engineering

ABSTRACT

Laser spectroscopy has been utilized to advance studies and efficiency in various fields such as energy, environment, and aerospace by providing quantitative, species-specific measurements of molecular temperature, pressure, and composition. For accurate measurements of those quantities, measured spectral data are often compared with standard calibrated databases. SpectraPlot is a web-based application that allows its users to simulate spectra and obtain calculations by sourcing from various databases including HITRAN, NIST, AD, and HITEMP. These databases have their own respective libraries of data regarding a large range of gaseous species at different conditions. The objective of this project is to create a relational database server with various spectroscopic databases and to develop application capabilities for broadband spectral simulations and line surveys. MySql was utilized as an efficient tool to manage databases with interconnected data tales and various different data types. In MySql, the server was configured, data was then uploaded as tables into their respective database within the server. When connected to the database server, the Python IDE was used to fetch data remotely and perform spectral simulations and surveys. Fetching data from the relational database is shown to be roughly four times faster (twenty times after connecting to the server), than reading data directly from local text files. Broadband line surveys were then conducted using data fetched from the server and linestrengths of different molecules within the wavenumber range of interest were plotted to provide visualization of results. Along with the line surveys, a hardware search on lasers was performed within the same wavenumber range of interest. The present work will help researchers target specific spectral regions of various species.

UCLA Samueli School of Engineering

Samueli Research Scholars

Development of SpectraPlot Application for Broadband Spectral Line Survey

Lizeth Vera, Chuyu Wei || PI: Professor R. Mitchell Spearrin
Laser Spectroscopy and Reacting Flows Laboratory
Department of Aerospace and Mechanical Engineering, University of California–Los Angeles

UCLA Samueli School of Engineering
SUMMER UNDERGRADUATE RESEARCH PROGRAM

Introduction

- Laser Spectroscopy studies how light is scattered or absorbed by a sample matter.
  - This allows one to study the structure of gaseous species' atoms and molecules.
- This form of studying sample matter has been used to advance studies and efficiency in various fields such as energy, environment, and aerospace by providing quantitative, species-specific measurements of molecular temperature, pressure, and composition.
- In order to acquire accurate measurements regarding sample matter, measured spectral data are compared with standard calibrated databases.

Objective

- SpectraPlot is a web-based application that allows its users to simulate spectra and obtain calculations by sourcing from various databases.
- These databases have their own respective libraries of data regarding a large range of gaseous species at different conditions.
- The objective of this project is to create a relational database server with various spectroscopic databases and to develop application capabilities for broadband spectral simulations and line surveys.

Materials and Methods

- **Software Used**
  - Relational Database Server (RDS) Software MySQL
    - MySql was utilized as an efficient tool to manage databases with interconnected data tables and various different data types
  - Python IDE Spyder
    - Used to fetch data remotely from servers and perform spectral simulations and surveys

- **Configure Server and Databases**
  - Set up local server with the necessary settings and security access
  - Create databases within server pertaining to the databases we are outsourcing information from
  - Within each database, assign a table to every species contained in the database
  - The tables should hold various information regarding the species at different conditions
- **Building Functionalities**
  - Link the databases in MySQL to Python IDE
  - Use a cursor in Spyder to access information held in server connected to
  - The cursor can execute MySQL commands to then fetch specific data from the database tables
  - Append information to an array if it fits our objectives
  - Plot all values within our arrays as data points on a stem plot graph

Results

MySQL Relational Schema

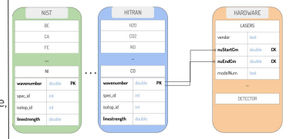

Figure 1. HITRAN , NIST, etc. databases hold tables of species' data with their primary key being *wavenumber*. The HARDWARE table has nuStartCm and nuEndCm columns which act as composite keys corresponding to the foreign key, *wavenumber*, in the species' tables.

Compared Fetch Times

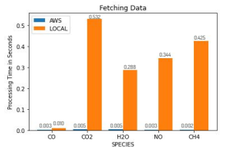

Figure 2. Compared the time taken to fetch data from various species' tables in Spyder using a connection to AWS and reading directly from the local text files

Broadband Line Survey

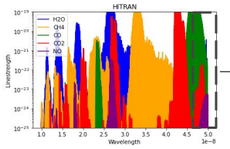

Figure 3. The linestrengths of 5 species from the HITRAN database were graphed within the wavenumber range of 2000-10000

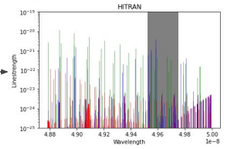

Figure 4. The range interest was focused in to 2000-2050, giving a closer look at how they interfere with one another. The shaded region is the wavenumber range of a laser compatible with the range of interest

Conclusion

- Relational database is created to manage various spectral database
- Fetching data from the relational database is shown to be about 4-200 times faster compared to reading the databases from local files, depending on table size
- Broadband line surveys were conducted using data fetched from the server and linestrengths of different molecules within the wavenumber range of interest which were plotted to provide visualization of the simulation results
- A hardware search on lasers was performed within the same wavenumber range of interest to help users pick optical hardwares

References and Acknowledgements

- Big thank you to the Laser Spectroscopy and Gas Dynamics Laboratory at UCLA
  - Goldenstein, C.S., Miller, V.A., Spearrin, R.M. and Strand, C.L., 2017. SpectraPlot. com: Integrated spectroscopic modeling of atomic and molecular gases. *Journal of Quantitative Spectroscopy and Radiative Transfer, 200*, pp.249-257

Kathleen Villasenor

Bioengineering
Sophomore, UCLA

Stabilized Self-Assembly of Polyelectrolyte Coacervate Droplets

FACULTY ADVISOR

Samanvaya Srivastava

DAILY LAB SUPERVISOR

Advait Holkar

DEPARTMENT

Chemical and Biomolecular Engineering

ABSTRACT

The controllable nature of coacervate polyelectrolyte complexes holds immense potential as an encapsulation and protection mechanism for proteins, drugs, and hereditary material in the human body. Two oppositely charged polyelectrolytes interact to make a complex in an aqueous solution and at high salt concentrations, these complexes take the form of coacervate liquid-phase droplets. The droplets tend to coalesce and sink to the bottom of the solution forming a polymer dense macro-phase. To increase the level of interaction of biological molecules with the complexes, the droplets must be stabilized and micro-phase separated in solution. Previously, weak polyelectrolyte complexes have been stabilized through the use of a graft polymer that interacts with the polyelectrolytes to give the complex an overall neutral charge. This experiment tested the same experimental design using strong polyelectrolytes, taking a closer look at the mechanisms behind complexation such as the effect of increasing salt concentration, varying the charge ratio of polyelectrolytes, shortening the polyelectrolyte chain length, and adding a graft polymer. To do so, the study employed PSS-Na, and PDADMAC, two oppositely charged polyelectrolytes. Salt was utilized to alter the level of electrostatic attraction to either promote or discourage precipitate complexation of the polyelectrolytes. The addition of a graft polymer with neutral offshoots was found to interact with the polyelectrolytes and disperse the complexes throughout the solution. The shortening of the polyelectrolyte chain weakened electrostatic interactions and lowered the degree of complexation, while charge ratio variation resulted in minimal changes to complexation tendencies. With an increased degree of control over polyelectrolyte complexation, the optimal concentration of polyelectrolytes, salt, and graft polymer was combined to yield a stabilized solution of polyelectrolyte complex coacervate droplets. This study demonstrates a method for stabilizing strong polyelectrolyte complex coacervates, and the success of the aforementioned experimental approach makes it viable for future stabilization attempts with precipitate and polyelectrolyte-protein complexes.

UCLA Samueli School of Engineering

Samueli Research Scholars

Stabilized Self-Assembly of Polyelectrolyte Coacervate Droplets

Kathleen Villasenor, Advait Holkar, Dr. Samanvaya Srivastava

Introduction:

The controllable nature of polyelectrolyte complexation holds immense potential as an encapsulation and delivery mechanism for proteins, drugs, and biological molecules. The following study takes a closer look at the mechanisms behind polyelectrolyte complexation such as the effect of increasing salt concentration, varying charge ratio, and adding a graft polymer.

Objective:

The goal of the following research is to investigate the optimal conditions for evenly dispersed coacervate polyelectrolyte complexes in order to stabilize the droplets in solution.

Future Applications: enable the creation of protein-polymer microparticles for the protection and storage of proteins.

Key Terms:

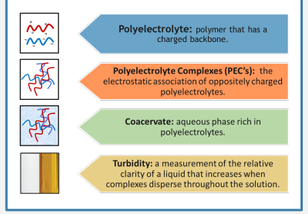

Materials:

1. **PSS-Na:** negatively charged strong polyelectrolyte
2. **PDADMAC:** positively charged strong polyelectrolyte
3. **Salt:** Potassium Bromide
4. **Graft Polymer:** a polymer with a charged backbone and neutral offshoots.

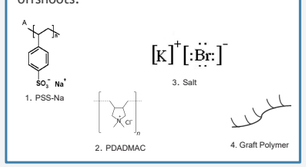

Experimental Design:

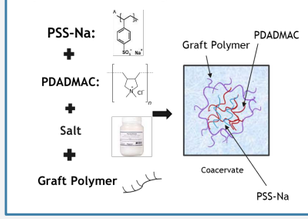

Tuning Polyelectrolyte Morphology:

1 The Variance of Charge Ratio

- Experimentation with different ratios of positively charged PDADMAC to negatively charged PSS-Na.

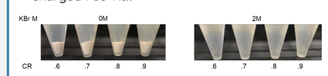

2 The Addition of Salt

- The addition of salt screens electrostatic interactions lowering the degree of complexation and inducing a solid to liquid phase transition in PECs.

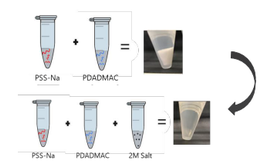

Lack of distinguishable difference with changes of charge ratio suggests that the charge offset has no observable effect on degree of complexation.

3 The Addition of Graft Polymer

- Glenium (GLE) was utilized as graft polymer to surround polyelectrolytes to give complex an overall neutral charge.

- Addition of GLE elevates solution turbidity indicating an increase in dispersion and stability of PECs

Finding the Optimal Salt Concentration:

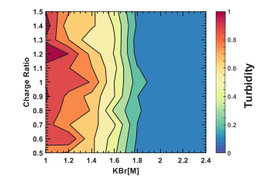

Experimental Conditions: 240 K PDADMAC, 70K PSS, varying KBR, H2O.

- 1.8M KBr is the added salt conc. at which most coacervate PEC's are present without precipitation (indicated by Turbidity > 0).

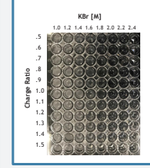

Supporting Data using 8.5 K PDADMAC:

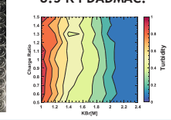

Stabilizing the Coacervates:

Experimental Conditions: 8.5 K PDADMAC, 70K PSS, 1.8 KBR, GLE.

The samples remain stable and uniformly dispersed for over 48 hours, indicating that the complexes are stabilized in solution.

Conclusion:

Our experiments characterize the driving factors of polyelectrolyte complexation and demonstrate a method for stabilizing strong polyelectrolyte complex coacervates in an aqueous solution.

Acknowledgements: I would like to thank the Srivastava Lab and the Samueli Summer Undergraduate Research Program for providing funding and guidance throughout this research endeavor.

Works Cited:

Li, Lu et al. "Effects Of Non-Electrostatic Intermolecular Interactions On The Phase Behavior Of Ph-Sensitive Polyelectrolyte Complexes". *Macromolecules*, 2020.

Sophie Wells

Civil Engineering
Freshman, UCLA

Can Satellites Actually Measure the Turbidity of the Water in Southern California

FACULTY ADVISOR

Jennifer Jay

DAILY LAB SUPERVISORS

Marisol Cira and Ileana Callejas

DEPARTMENT

Civil and Environmental Engineering

ABSTRACT

Turbidity is the measurement of how much light passes through a liquid. Turbidity is important to study as particles in turbid water can act as vectors to bacteria. In this study, images taken from the Sentinel-2 satellite measured the turbidity of beaches around Los Angeles. First, we compared satellite-derived turbidity from the Nechad algorithm to in situ turbidity samples, then turbidity was compared to Fecal Indicator Bacteria. This experiment was split up into three parts: first, the total suspended solids (TSS) test, measuring how many particles are in a sample. Second, the fecal indicator bacteria (FIB) test, measuring the probability of how much bacteria is in 100mL of the sample. Lastly, Google Earth Engine (GEE), a cloud-based platform for planetary-scale geospatial analysis, calculated turbidity from the Sentinel-2 satellite. After collecting water samples from Los Angeles beaches for in situ TSS and FIB tests, the correlation was found to be low (R2=0.2), suggesting that the clarity of the water does not translate to how much bacteria was in the sample. Yet, there was a correlation between in-lab TSS and the Turbidity from Sentinel-2 (R2=0.8), indicating that Sentinel-2 accurately measured turbidity. In the future, research should be done to compare TSS from different algorithms, satellites, and different beaches. This would have a major impact on society as satellites would be able to detect whether water is safe to recreate in.

UCLA Samueli School of Engineering

Can Satellites Actually Measure the Turbidity of the Water in Southern California

Sophie Wells, Yuwei Kong, Marisol Cira, Ileana Callejas, Professor Jennifer Jay
Department of Civil and Environmental Engineering, University of California -- Los Angeles

Samueli Research Scholars

UCLA Samueli School of Engineering
SUMMER UNDERGRADUATE RESEARCH PROGRAM

Abstract

Turbidity is the measurement of how much light passes through a liquid. Turbidity is important to study as particles in turbid water can act as vectors to bacteria. In this study, images taken from the Sentinel-2 satellite measured the turbidity of beaches around Los Angeles. First, we compared satellite-derived turbidity from the Nechad algorithm to in situ turbidity samples, then turbidity was compared to Fecal Indicator Bacteria. This experiment was split up into three parts: first, the total suspended solids (TSS) test, measuring how many particles are in a sample. Second, the fecal indicator bacteria (FIB) test, measuring the probability of how much bacteria is in 100mL of the sample. Lastly, Google Earth Engine (GEE), a cloud-based platform for planetary-scale geospatial analysis, calculated turbidity from the Sentinel-2 satellite.

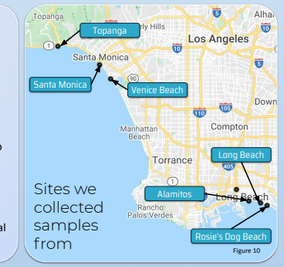

Figure 10

Results

Part 1 - Total Suspended Solid (TSS)

We noticed that after averaging each one of the tss data for each filter, we got the data seen in Figure 11. (the * are control filters that we filtered distilled water so we know we are filtering properly) We decided to only take into account the data I collected on July 22nd, 2021.

Date Collected	Site	TSS Average (mg/L)
7/22/21	SM1	14.3333
7/22/21	SM2	
7/22/21	SM3	
7/22/21	VB1	10.6667
7/22/21	VB2	
7/22/21	VB3	
7/22/21	AB1	27.1111
7/22/21	AB2	
7/22/21	AB3	
7/22/21	LB1	87.6667
7/22/21	LB2	
7/22/21	LB3	
7/22/21	DB1	44.3333
7/22/21	DB2	
7/22/21	DB3	
7/22/21	*1	0
7/22/21	*2	

Figure 11

Key:
VB = Venice Beach
SM = Santa Monica Beach
DB = Rosies Dog Beach
AB = Alamedos Beach
LB = Long Beach City Beach
* = Control (Distilled Water)

Part 2 - Fecal Indicator Bacteria (FIB)

For each site, there was different values for Total Coliform (Fig. 12), *E. Coli* (Fig. 13) and *Enterococcus* (Fig. 14).

Date	Site	(MPN/100mL)*Dilution
7/22/2021	SM	74
7/22/2021	VB	657
7/22/2021	LB	327
7/22/2021	DB	75
7/22/2021	AB	7270

Figure 12 - TC

Date	Site	(MPN/100mL)*Dilution
7/22/2021	SM	10
7/22/2021	VB	10
7/22/2021	LB	52
7/22/2021	DB	109
7/22/2021	AB	30

Figure 13 - EC

Date	Site	(MPN/100mL)*Dilution
7/22/2021	SM	0
7/22/2021	VB	0
7/22/2021	LB	0
7/22/2021	DB	41
7/22/2021	AB	146

Figure 14 - ENT

Part 3 - Google Earth Engine

Also known as the ORCAA tool, I simply pressed a black point seen on Figure 10, and as Figure 9 shows, it gave me the turbidity circled in red.

Site	Date	ORCAA Turb (NTU)
SM	7/22/21	2.744664345
VB	7/22/21	3.850354287
AB	7/22/21	4.139171672
LB	7/22/21	6.369673523
DB	7/22/21	4.14109737

Figure 15

Part 4 - Final Data

We noticed that there was a correlation (R^2=.8) meaning that the satellite can accurately measure that the water was not clear (Fig. 16). However, after correlating the TSS with the FIB (Fig 17-19), there wasn't a correlation. This means that murky water doesn't necessarily mean a lot of bacteria in it. So satellites can measure turbidity but not the bacteria.

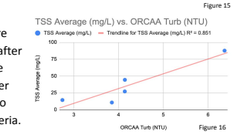

Figure 16

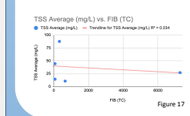

Figure 17

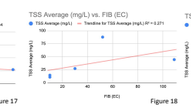

Figure 18

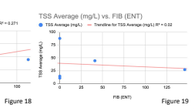

Figure 19

Materials/Methods

This experiment was split up into three parts:

Part 1 - Total Suspended Solid (TSS)

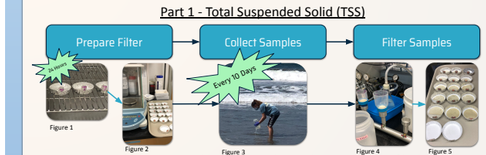

Figure 1 Figure 2 Figure 3 Figure 4 Figure 5

To prepare the filter, I put it in the oven for 24 hours, then weighed the filters. We collected water samples from LA beaches on August 22nd, 2021 (when the Sentinel-2 satellite passed over). Then after filtering the beach samples, I weighed the filters again. To get the total suspended solid (mg/L), I did the equation (Fig. 6) then took the average of the answer to get the average total suspended solid per site.

$$\frac{weight\ after\ (g) - weight\ before\ (g)}{volume\ added}$$

0.000001

Figure 6

Part 2 - Fecal Indicator Bacteria (FIB)

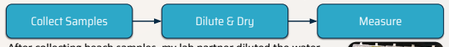

After collecting beach samples, my lab partner diluted the water sample, added IDEXX Quanti-Tray® bacteria indicator, then dried out the samples. After taking it out of the oven, we counted the number of big and small yellow squares to calculate the probability of coliforms in the water. Then, we put the trays under the UV light and counted the number of big and small illuminated squares to calculate the probability of *E. Coli* in the sample.

Figure 7

Figure 8

Part 3 - Google Earth Engine (GEE)

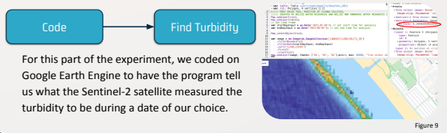

For this part of the experiment, we coded on Google Earth Engine to have the program tell us what the Sentinel-2 satellite measured the turbidity to be during a date of our choice.

Figure 9

Conclusion

After collecting water samples from Los Angeles beaches for in situ TSS and FIB tests, the correlation was found to be low (R2=0.2), suggesting that the clarity of the water does not translate to how much bacteria was in the sample. Yet, there was a correlation between in-lab TSS and the Turbidity from Sentinel-2 (R2=0.8), indicating that Sentinel-2 accurately measured turbidity. In the future, research should be done to compare TSS from different algorithms, satellites, and different beaches. This would have a major impact on society as satellites would be able to detect whether water is safe to recreate in.

Acknowledgement

I would like to thank the Summer Undergraduate Research Program, my professor Jennifer Jay, my daily lab supervisor Ileana Callejas, and my lab partner Yuwei Kong for their help and support on my research.

References

Callejas, Ileana A., Christine M. Lee, Deepak R. Mishra, Stacey L. Felgate, Claire Evans, Abel Carrias, Andria Rosado, Robert Griffin, Emil A. Cherrington, Mariam Ayad, Megha Rudresh, Benjamin P. Page, and Jennifer A. Jay. "Effect of COVID-19 Anthropause on Water Clarity in the Belize Coastal Lagoon." *Frontiers*. Frontiers, 12 Apr. 2021. Web. 08 July 2021.
"Notes from the Field - On the Ground in Belize to Improve How Satellites "See" Water Quality from Space." *NASA*. NASA. Web. 08 July 2021.
Steele, Jim. "Study of How COVID Tourism Decline Affects Belize's Coastal Waters Earns NASA Grant." *The University of Alabama in Huntsville*. The University of Alabama in Huntsville, 24 Sept. 2020. Web. 08 July 2021.
Written by Brian Spaen, Writer for Green Matters. "Belize's Barrier Reef Is No Longer Endangered." *World Economic Forum*. Web. 08 July 2021.

Lime Yao

Computer Engineering
Freshman, UCLA

Courtney Gibbons

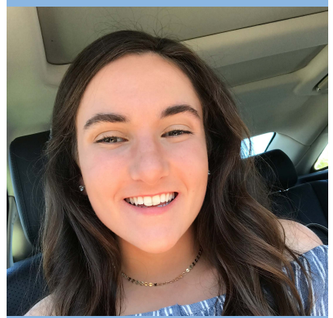

Electrical Engineering
Freshman, UCLA

Verifying Conditions for Magnetic Alignment in Canine Urination and Defecation with Citizen Science Dataset

FACULTY ADVISOR

Clarice Aiello

DAILY LAB SUPERVISOR

João Carlos Ribeiro-Silva

DEPARTMENT

Electrical and Computer Engineering

ABSTRACT

Numerous species of animals are known to have magnetoreception, or the ability to detect the Earth's magnetic field, for orientation and navigation. However, more research is needed to confirm the underlying mechanics of magnetoreception in animals. Compelling evidence has suggested that dogs align to the Earth's magnetic field during excremental activity if the nearby magnetic field declination, or the difference between true north and magnetic north, is stagnant. Nonetheless, this phenomenon needs a robust source of experimental data before it can be established. We are compiling a large image dataset of urinating and defecating dogs with citizen science and automating the analysis of geomagnetic metadata embedded within these images. We hope to verify whether canine alignment in urination and defecation depends on magnetic field declination. Initial results from a low sample size indicate dogs face random directions even when the percent change magnetic field declination is less than 1%. However, the project will require more image submissions from across the world to yield more refined results. If dogs demonstrate magnetoreception in the course of this project, their potential role as experimental subjects will be pivotal in developing future magnetoreception research.

UCLA Samueli School of Engineering

Previous research suggests **dogs align** with the **Earth's magnetic field** when they **urinate and defecate** if the **magnetic field declination** is **stagnant** at that point in space and time.

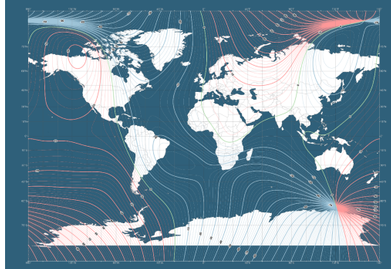

World magnetic model of main field declination, the difference between true North and magnetic North, in 2020 [2]. The green curves represent 0 magnetic field declination; the red curves represent positive magnetic field declination, indicating magnetic north is east of true north; and the blue curves represent negative magnetic field declination, indicating magnetic north is west of true north. The thicker curves occur every 10° magnetic north and true north vary from each other.

We seek to establish or refute this fact by **increasing the sample size** with **citizen science** and deploying **metadata extraction** and **automated analysis**.

Scan this to view our website & submit your dog photos!

Verfiying Conditions for Magnetic Alignment in Canine Urination and Defecation with Citizen Science Dataset

Courtney A. Gibbons, Lime Yao, Gina Talcott, Josh Cielo, Greg Damelin, Clarice D. Aiello
Department of Electrical and Computer Engineering, University of California – Los Angeles

Important Concepts

- **Magnetoreception:** the ability to detect the Earth's magnetic field.
- **Magnetic field declination:** the difference between true north and magnetic north.
- **Exif metadata:** information embedded in an image, such as geolocation and camera specifications.
- **Citizen science:** when the general public participates in scientific research, often by providing data.

Researching Magnetoreception in Dogs

- Previous research suggests **dogs have magnetoreception** and **align with the Earth's magnetic field during excremental activity** when the **magnetic field declination is stagnant** [1].
- With a sample size of only 70 dogs located in rural parts of Germany and the Czech Republic, **more research and data is needed** [1].
- We aim to expand the sample size by **compiling a large image dataset** of urinating and defecating dogs with **citizen science** and analyzing the **geomagnetic metadata** embedded within these images.
- We hope to **verify whether canine alignment in urination and defecation depends on magnetic field declination and environment.**

Fully Automated Image Collection Process

- We asked dog owners to take pictures **from behind their dog**, effectively **measuring the dog's magnetic orientation** like a compass would, when their dog was urinating or defecating.

Lab Social Accounts & Website
Obtain images of urinating & defecating dogs from participating dog owners.

Google Script
Sort photos based on environmental keywords.

Exif Metadata Extraction
Retrieve photo direction & GPS data.

Calculate Magnetic Field Declination
Use GPS data & NOAA calculator [2].

Analysis
Average direction across all dogs and correlate various factors that encourage or discourage magnetic alignment:
- Magnetic declination change
- Rural vs urban environment

Preliminary Results with a Low Sample Size

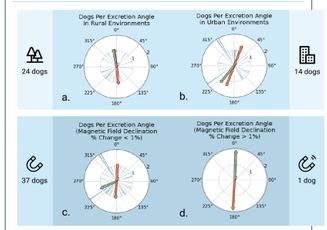

- Circular bar plots of **excretion angles east of north** are sorted by **rural (a)** versus **urban environments (b)** and **rate of magnetic field declination change below (c)** and **above (d) %1**.
- Red vectors indicate **average excretion axis**, and green vectors indicate **average excretion direction**. Vector **magnitudes** represent the **extent of dogs' preference for magnetic alignment** towards that direction.
- This preliminary data consisted of only 38 dog images, and the dogs of the current dataset exhibited **no preference for a particular angle** and faced in random directions.

Future Prospects and Simulations

- This project will require **more image submissions from across the world** to yield more refined results.
- **Simulated plots** indicate the desired result of this project: data from many dogs that allow us to **establish or refute if dogs align with the Earth's magnetic field when they urinate and defecate**.
- Other future prospects include:
  - **Update plots on our website** every time a new photo is submitted
  - **Engage the community** by featuring dogs that have contributed to our study
- If dogs demonstrate magnetoreception in the course of this study, their potential role as experimental subjects will be pivotal in developing **future magnetoreception research**.

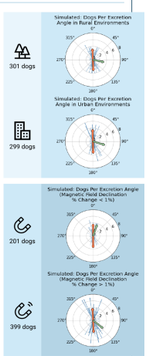

References and Acknowledgements

- [1] Hart et al.: Dogs are sensitive to small variations of the Earth's magnetic field. Frontiers in Zoology 2013 10:80
- [2] NCEI Geomagnetic Calculators: Magnetic Delincation Estimated Value. National Oceanic and Atmospheric Administration. https://www.ngdc.noaa.gov/geomag/ calculators/magcalc.shtml

- We would like to thank the National Science Foundation (NSF), the UCLA Summer Undergraduate Research Program (SURP), and the UCLA Fast Track to Success program for this research opportunity. We also thank Professor Clarice Aiello for her knowledge and support.

UCLA Samueli School of Engineering SUMMER UNDERGRADUATE RESEARCH PROGRAM
FAST TRACK TO SUCCESS UCLA Electrical and Computer Engineering
QuBiT

Ivy Zhang

Electrical Engineering
Freshman, UCLA

Tiffany Tsou

Electrical Engineering
Freshman, UCLA

Solving Large-Scale Non-metric Multidimensional Scaling Problems Using ADMM Optimization

FACULTY ADVISOR

Lieven Vandenberghe

DAILY LAB SUPERVISOR

Xin Jiang

DEPARTMENT

Electrical and Computer Engineering

ABSTRACT

Analysis of the relative orderings of the differences between model predictions as opposed to a quantitative method is often required in cases such as customers expressing their preferences instead of giving numerical scores. The purpose of this research project is to use an algorithm based on the alternating direction method of multipliers (ADMM) to solve large-scale non-metric multidimensional scaling (NMDS) problems. The NMDS problem seeks to optimize the Gram matrix of the calculated position vectors by minimizing violations of the inequality constraints that express the ordering relations of their pairwise distances. ADMM is a method for large-scale optimization which splits variable x into two parts and performs alternating optimizations over each part. The problem is coded using Python and Matlab, allowing us to see what fraction of the ordering of the original distances is preserved. We are working with randomly generated datasets. We are also working with more interesting data, including Swiss Roll and S curve data generated using Python, and real-world data such as sets of related images. For our initial results, which did not include any code for ADMM, the fraction of the ordering of distances preserved was quite high, indicating that the relative ordering of the original distances was preserved overall.

UCLA Samueli School of Engineering

Solving Large Scale Non-metric Multidimensional Scaling Problems Using ADMM Optimization

Tiffany Tsou and Ivy Zhang
Professor Lieven Vandenberghe, Xin Jiang, Taylor Chung

Samueli Research Scholars

UCLA Samueli School of Engineering
SUMMER UNDERGRADUATE RESEARCH PROGRAM

INTRODUCTION + OBJECTIVE

The goal of this research project is to use an algorithm based on the alternating direction method of multipliers (ADMM), to solve large-scale non-metric multidimensional scaling (NMDS) problems with randomly generated datasets and more interesting and real-world datasets such as the Swiss roll, S curve, and related images. Our hypothesis is that the calculated Gram matrix will preserve the ordering of the original distances between points in our initial dataset.

PRINCIPLES

NMDS: attempts to preserve the original distances between inputs in a dataset.
ADMM: a method for large-scale optimization which performs alternating optimizations over two vector variables x and y.
Convex optimization: a convex objective function is subject to inequality constraints that are summarized by a slack variable that we seek to minimize.

Figures: S curve and Swiss roll.

Source: https://www.semanticscholar.org/paper/Nonlinear-Manifold-Learning-6-.-454-Summary-Ihler/62bc7f7507f8f3e7c9c4ac62215d31b06e45da98/figure/0

MATERIALS

Python: Optimization package cvxpy
Matlab: Optimization package CVX
Datasets: Random datasets of size 50, Swiss roll dataset, S curve dataset, images

METHODS

1. Generate datasets with random data points, Swiss roll, S curve, images.
2. Code optimization problem along with ADMM solution into Python and then into Matlab.
3. Analyze results in Python and Matlab.
4. Make necessary adjustments to code and repeat.

$$\begin{aligned} \min_{K,\xi_{ijkl}} \quad & \sum_{(i,j,k,l)\in\mathcal{S}} \xi_{ijkl} + \lambda \operatorname{Trace}(K) \\ \text{subject to} \quad & k_{kk} - 2k_{kl} + k_{ll} - k_{ii} + 2k_{ij} - k_{jj} \geq 1 - \xi_{ijkl} \\ & \sum_{ab} k_{ab} = 0, \quad K \succeq 0. \qquad \text{(GNMDS)} \end{aligned}$$

This is the optimization problem with inequality constraints represented as linear equations of Gram matrix K which define a unique K which can solve the problem and have specifications that disallow translations, rotations, and scalings of K.
Source: Agarwal et al.

$$\begin{aligned} \text{minimize} \quad & \sum_{k=1}^{m} \max\{0, u_k\} + \lambda \mathbf{1}^T x + g(x) + h(y) \\ \text{subject to} \quad & \begin{bmatrix} I & 0 \\ 0 & I \end{bmatrix} \begin{bmatrix} x \\ u \end{bmatrix} + \begin{bmatrix} -I \\ -A \end{bmatrix} y = \begin{bmatrix} 0 \\ \mathbf{1} \end{bmatrix}. \end{aligned}$$

This is the optimization problem in an ADMM-ready form, which consists of first optimization over x and u, then optimization over y, and lastly the dual update. Source: Boyd et al.

RESULTS

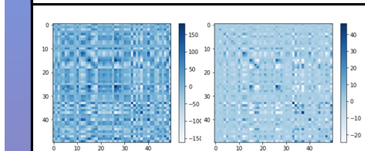

Figure: Shows the original Gram matrix calculated from the original distances matrix (left) and the calculated Gram matrix obtained by solving the non-metric multidimensional scaling problem (right).

Figure: Shows the values of the slack variable (error); ordering of distances is overall preserved.

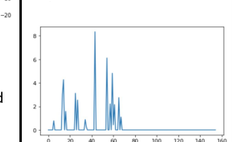

REFERENCES

Agarwal, S., Wills, J., Cayton, L., Lanckriet, G., Kriegman, D., & Belongie, S. (2007, March). Generalized non-metric multidimensional scaling. In Artificial Intelligence and Statistics (pp. 11-18). PMLR.
Boyd, S., Parikh, N., & Chu, E. (2011). Distributed optimization and statistical learning via the alternating direction method of multipliers. Now Publishers Inc.

ACKNOWLEDGEMENTS

We would like to thank the Summer Undergraduate Research Program for providing the guidance and resources to succeed with this project, Professor Lieven Vandenberghe, Xin Jiang, and Taylor Chung for providing their knowledge and resources, and NSF for funding this project.

Jolin Zhang

Computer Engineering
Freshman, UCLA

Trung Vong

Computer Science
Sophomore, East Los Angeles College

Rudy Orre

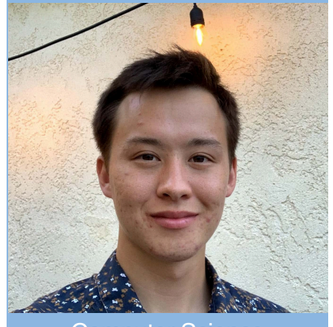

Computer Science
Sophomore, El Camino College

Reinforcement Learning in an Imperfect Information Game

FACULTY ADVISOR

Gregory Pottie

DAILY LAB SUPERVISORS

Sunay Bhat, Jeffrey Jiang

DEPARTMENT

Electrical and Computer Engineering

ABSTRACT

Reinforcement learning (RL) has been a growing subset of machine learning with increasing success and promise - but it has just begun to be used in complex, multiplayer environments and games. An agent learns in a complex environment through trial and error, beginning from fully random trials and finishing with sophisticated actions. We apply RL to the imperfect information game known as Liar's Dice, which presents a challenging mix of two-player dynamics and partial information to explore. The game forces players to call bluffs and doubt opponents while reading others' potential actions. Implementing reinforcement learning to imperfect information games allows us to find successful strategies and models in dynamic Markov Decision Process (MDP) environments that require sequential decision making. Utilizing both Python and MATLAB, we employed the popular Q-learning method of RL to train agents that begin with random actions or to use a combination of fixed strategies against others. An agent employing Q-learning improved its win rate from 50% to only 65% within 1,000,000 episodes against a simple agent. On the other hand, an agent that made decisions based on various fixed strategies available increased its win rate from 11% to 77.7% with 100,000 episodes. Those varying speeds demonstrate the difficulty of learning and the variability of Q-learning in a game with partial information. In future work, we may compare counterfactual regret minimization and more state-of-the-art RL algorithms, which would expand our understanding of various methods of a partially observed, dynamic environment such as Liar's Dice. By studying this game, we hope to one day broaden our results to the education space, a similar Markov process where individuals also make decisions sequentially. Using intervention tools such as quizzes and lectures, the interactions between students and instructors may be refined to improve student learning outcomes.

UCLA Samueli School of Engineering

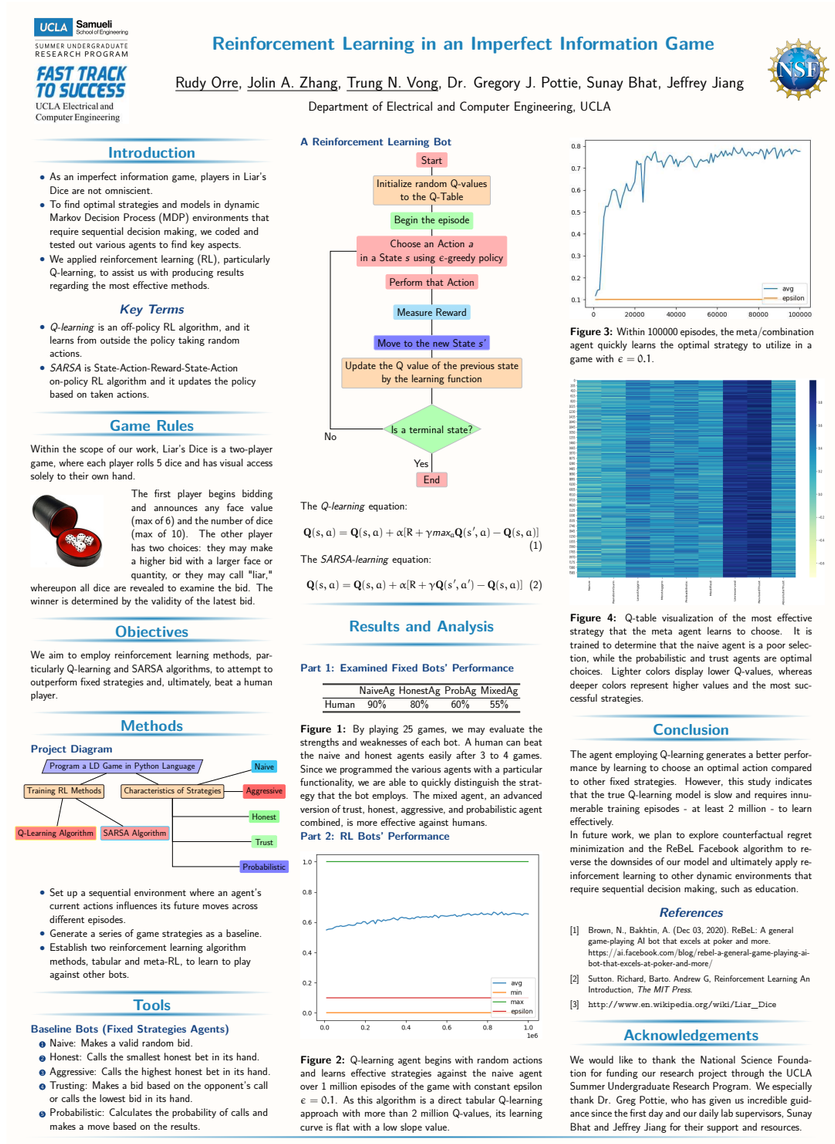

UCLA Samueli School of Engineering
SUMMER UNDERGRADUATE RESEARCH PROGRAM
FAST TRACK TO SUCCESS
UCLA Electrical and Computer Engineering

Reinforcement Learning in an Imperfect Information Game

Rudy Orre, Jolin A. Zhang, Trung N. Vong, Dr. Gregory J. Pottie, Sunay Bhat, Jeffrey Jiang
Department of Electrical and Computer Engineering, UCLA

Introduction
- As an imperfect information game, players in Liar's Dice are not omniscient.
- To find optimal strategies and models in dynamic Markov Decision Process (MDP) environments that require sequential decision making, we coded and tested out various agents to find key aspects.
- We applied reinforcement learning (RL), particularly Q-learning, to assist us with producing results regarding the most effective methods.

Key Terms
- *Q-learning* is an off-policy RL algorithm, and it learns from outside the policy taking random actions.
- *SARSA* is State-Action-Reward-State-Action on-policy RL algorithm and it updates the policy based on taken actions.

Game Rules
Within the scope of our work, Liar's Dice is a two-player game, where each player rolls 5 dice and has visual access solely to their own hand.
The first player begins bidding and announces any face value (max of 6) and the number of dice (max of 10). The other player has two choices: they may make a higher bid with a larger face or quantity, or they may call "liar," whereupon all dice are revealed to examine the bid. The winner is determined by the validity of the latest bid.

Objectives
We aim to employ reinforcement learning methods, particularly Q-learning and SARSA algorithms, to attempt to outperform fixed strategies and, ultimately, beat a human player.

Methods
Project Diagram
Program a LD Game in Python Language; Training RL Methods; Characteristics of Strategies; Q-Learning Algorithm; SARSA Algorithm; Naive; Aggressive; Honest; Trust; Probabilistic
- Set up a sequential environment where an agent's current actions influences its future moves across different episodes.
- Generate a series of game strategies as a baseline.
- Establish two reinforcement learning algorithm methods, tabular and meta-RL, to learn to play against other bots.

Tools
Baseline Bots (Fixed Strategies Agents)
1. Naive: Makes a valid random bid.
2. Honest: Calls the smallest honest bet in its hand.
3. Aggressive: Calls the highest honest bet in its hand.
4. Trusting: Makes a bid based on the opponent's call or calls the lowest bid in its hand.
5. Probabilistic: Calculates the probability of calls and makes a move based on the results.

A Reinforcement Learning Bot
Start → Initialize random Q-values to the Q-Table → Begin the episode → Choose an Action a in a State s using ϵ-greedy policy → Perform that Action → Measure Reward → Move to the new State s' → Update the Q value of the previous state by the learning function → Is a terminal state? No / Yes → End

The *Q-learning* equation:
$$\mathbf{Q}(s,a) = \mathbf{Q}(s,a) + \alpha[R + \gamma max_a \mathbf{Q}(s',a) - \mathbf{Q}(s,a)] \quad (1)$$
The *SARSA-learning* equation:
$$\mathbf{Q}(s,a) = \mathbf{Q}(s,a) + \alpha[R + \gamma \mathbf{Q}(s',a') - \mathbf{Q}(s,a)] \quad (2)$$

Results and Analysis
Part 1: Examined Fixed Bots' Performance

	NaiveAg	HonestAg	ProbAg	MixedAg
Human	90%	80%	60%	55%

Figure 1: By playing 25 games, we may evaluate the strengths and weaknesses of each bot. A human can beat the naive and honest agents easily after 3 to 4 games. Since we programmed the various agents with a particular functionality, we are able to quickly distinguish the strategy that the bot employs. The mixed agent, an advanced version of trust, honest, aggressive, and probabilistic agent combined, is more effective against humans.
Part 2: RL Bots' Performance
Figure 2: Q-learning agent begins with random actions and learns effective strategies against the naive agent over 1 million episodes of the game with constant epsilon $\epsilon = 0.1$. As this algorithm is a direct tabular Q-learning approach with more than 2 million Q-values, its learning curve is flat with a low slope value.

Figure 3: Within 100000 episodes, the meta/combination agent quickly learns the optimal strategy to utilize in a game with $\epsilon = 0.1$.
Figure 4: Q-table visualization of the most effective strategy that the meta agent learns to choose. It is trained to determine that the naive agent is a poor selection, while the probabilistic and trust agents are optimal choices. Lighter colors display lower Q-values, whereas deeper colors represent higher values and the most successful strategies.

Conclusion
The agent employing Q-learning generates a better performance by learning to choose an optimal action compared to other fixed strategies. However, this study indicates that the true Q-learning model is slow and requires innumerable training episodes - at least 2 million - to learn effectively.
In future work, we plan to explore counterfactual regret minimization and the ReBeL Facebook algorithm to reverse the downsides of our model and ultimately apply reinforcement learning to other dynamic environments that require sequential decision making, such as education.

References
[1] Brown, N., Bakhtin, A. (Dec 03, 2020). ReBeL: A general game-playing AI bot that excels at poker and more. https://ai.facebook.com/blog/rebel-a-general-game-playing-ai-bot-that-excels-at-poker-and-more/
[2] Sutton. Richard, Barto. Andrew G, Reinforcement Learning An Introduction, *The MIT Press*.
[3] http://www.en.wikipedia.org/wiki/Liar_Dice

Acknowledgements
We would like to thank the National Science Foundation for funding our research project through the UCLA Summer Undergraduate Research Program. We especially thank Dr. Greg Pottie, who has given us incredible guidance since the first day and our daily lab supervisors, Sunay Bhat and Jeffrey Jiang for their support and resources.

UCLA Symposium Conference, August 28, 2021, California, USA

SURP is an umbrella program that administers and scaffolds summer undergraduate research opportunities within UCLA Samueli Engineering. SURP participating sub-programs include National Science Foundation (NSF) Research Experience for Undergraduates (REU) Sites, Samueli Research Scholars (SRS) Program, Faculty-funded grants, and Electrical and Computer Engineering Fast Track Program.

William Herrera, the director of SURP, is also director of UCLA Samueli Engineering's Undergraduate Research and Internship Program (URP/UIP) during the academic year. URP/UIP is committed to helping you find research/internship opportunities. Our Peer Advisors are trained to help you with any questions and concerns you may have, and appointments are available on our website.

For any questions about these resources, please reach out to us at urp@seas.ucla.edu and uip@seas.ucla.edu, or scan the QR code on the next page to get to our website.

We also encourage you to follow us on social media to stay updated on future professional development event and opportunities.

seasoasa.ucla.edu/undergraduate-research-program/

Samueli Engineering Undergraduate Research and Internship Program

UCLA Samueli Undergraduate Internship Program

UCLA Engineering Internship and Research Program

samueliurpuip

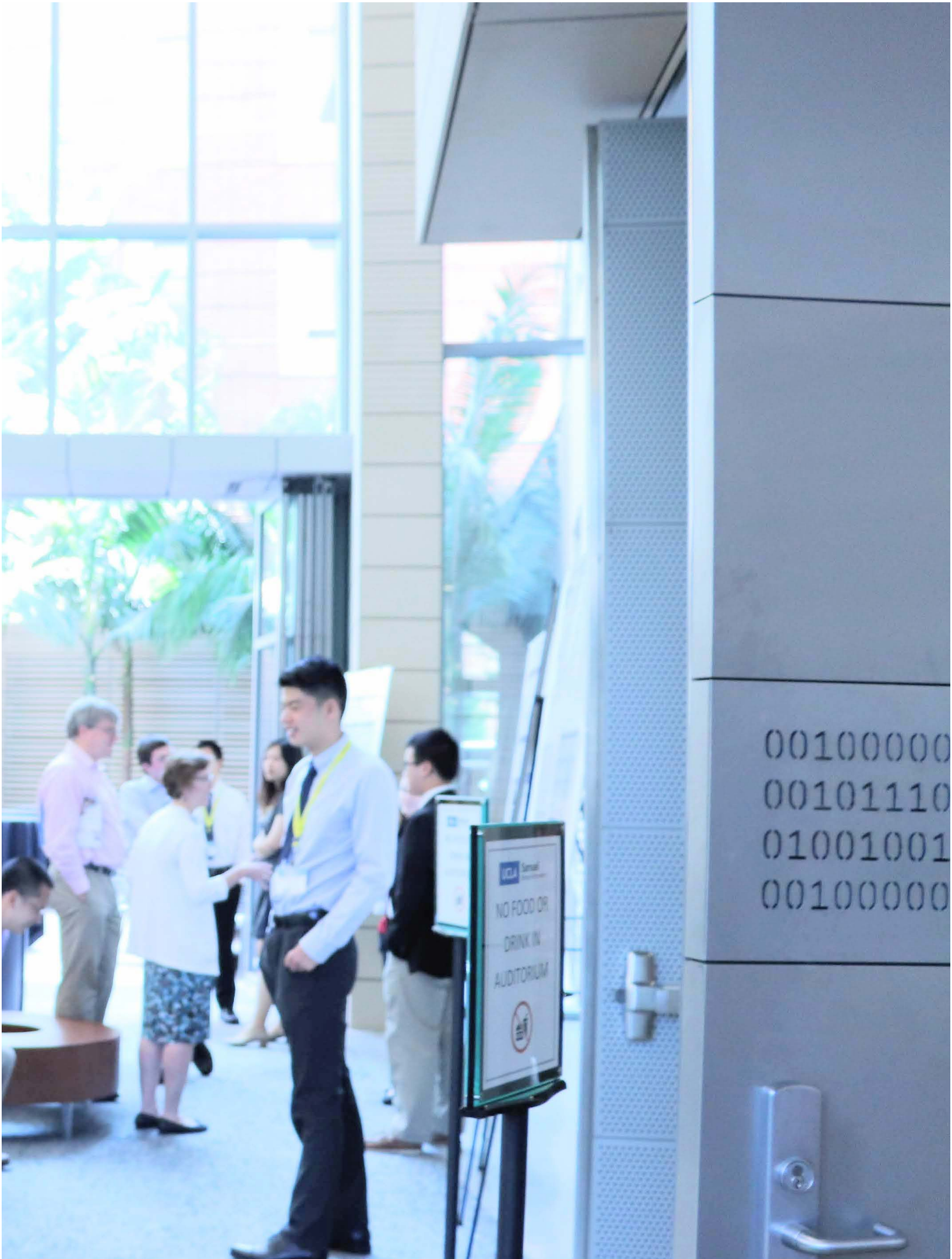
NO FOOD OR
DRINK IN
AUDITORIUM
00100000
00101110
01001001
00100000